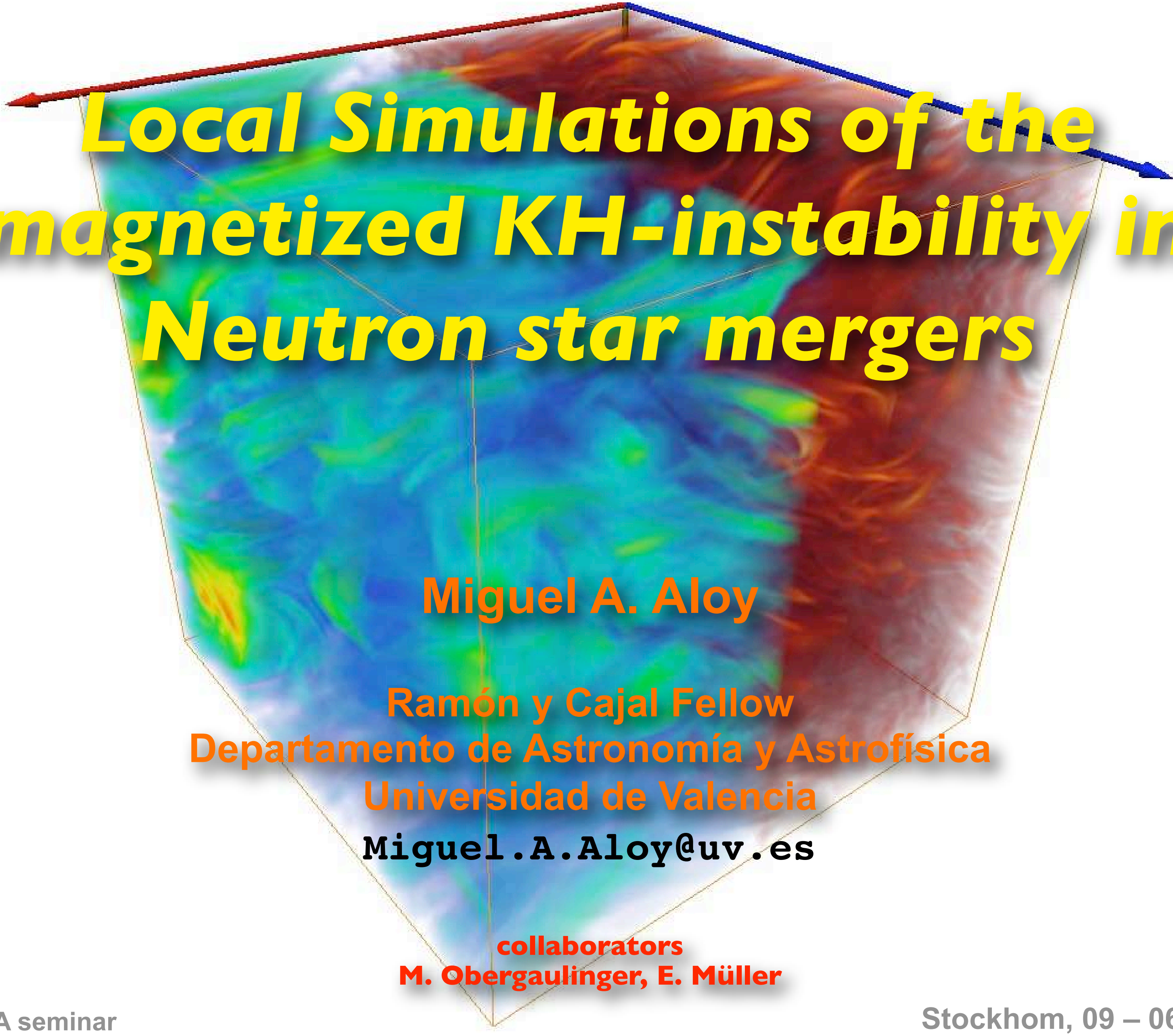

Local Simulations of the magnetized KH-instability in Neutron star mergers

Miguel A. Aloy

Ramón y Cajal Fellow
Departamento de Astronomía y Astrofísica
Universidad de Valencia
Miguel.A.Aloy@uv.es

collaborators
M. Obergaulinger, E. Müller

NORDITA seminar

Stockhom, 09 – 06 - 2009

Setting the stage

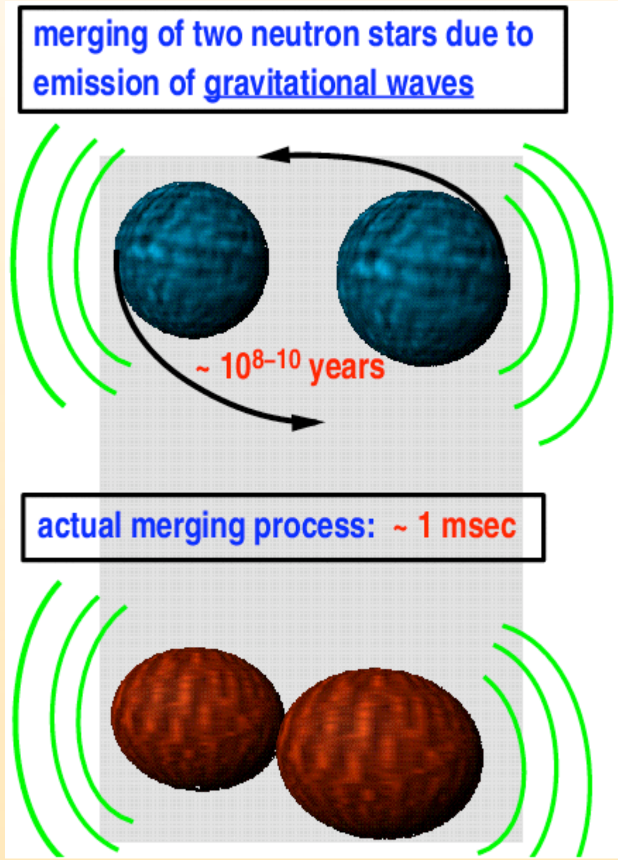

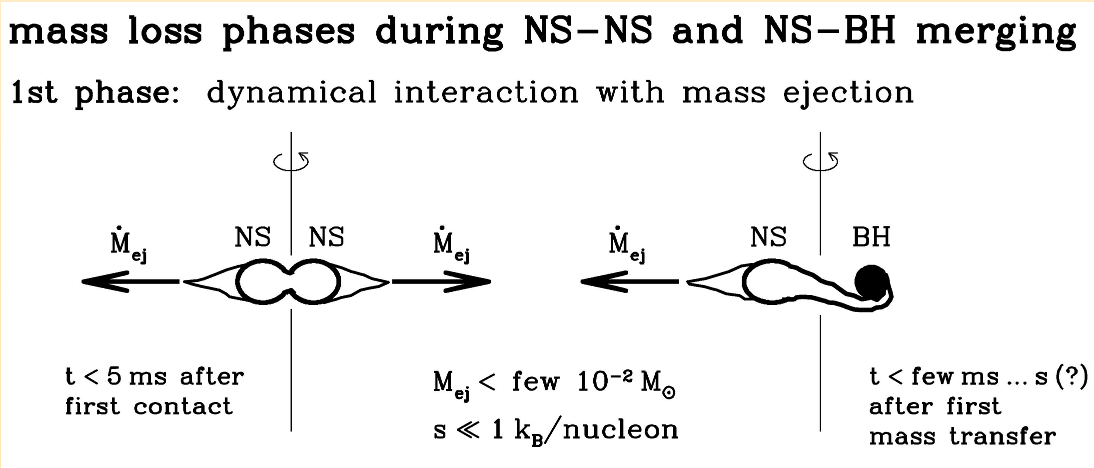

Setting the stage

— The merger of two neutron stars is considered the most promising scenario for the generation of short GRBs.

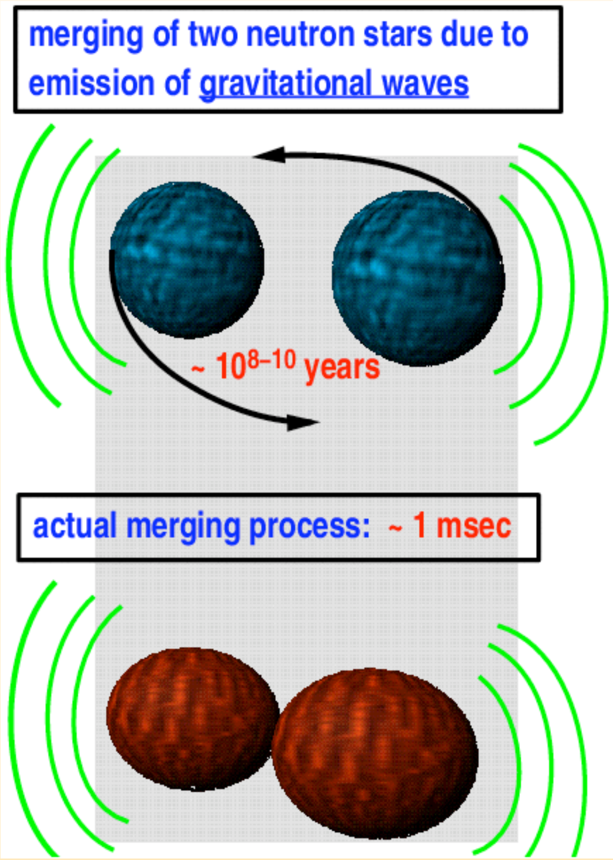

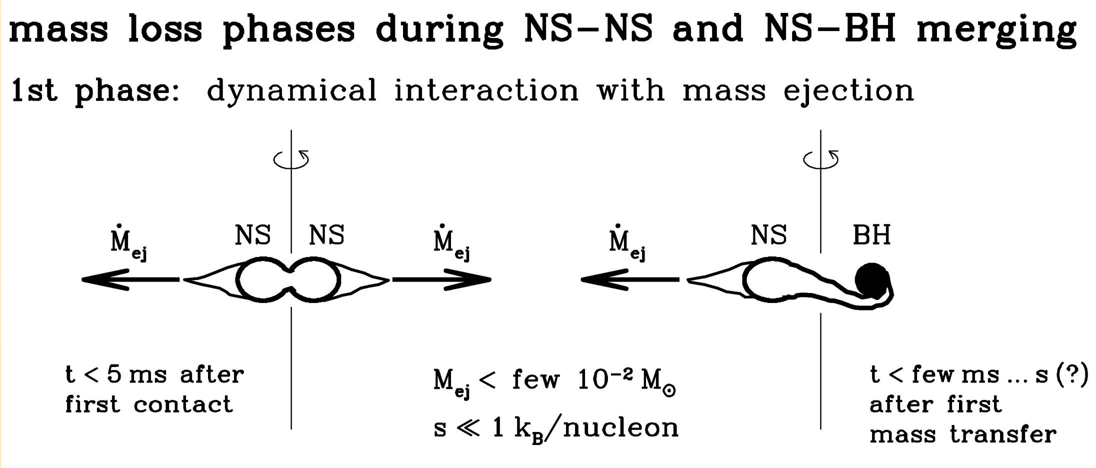

Setting the stage

- The merger of two neutron stars is considered the most promising scenario for the generation of short GRBs.
- After a phase of inspiral due to the loss of angular momentum and orbital energy by gravitational radiation, the merging NSs are distorted by their mutual tidal forces.

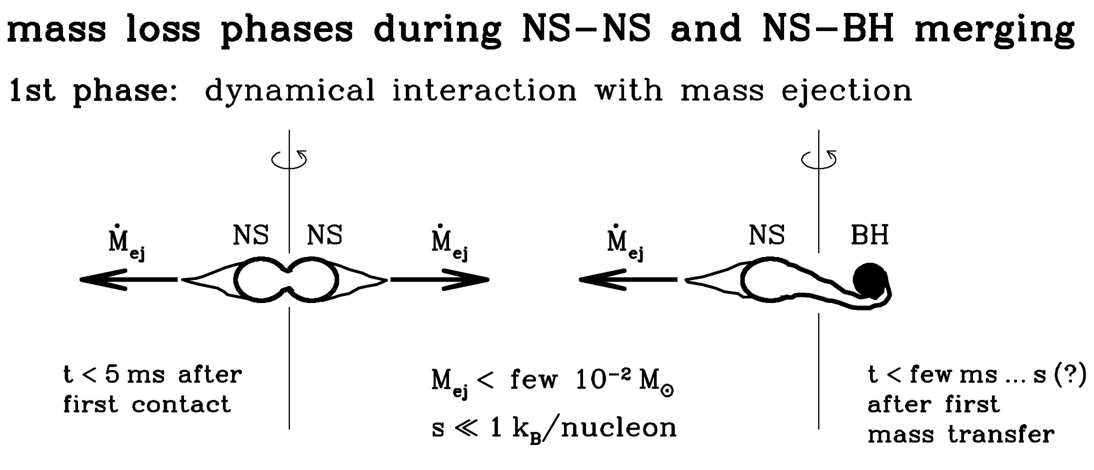

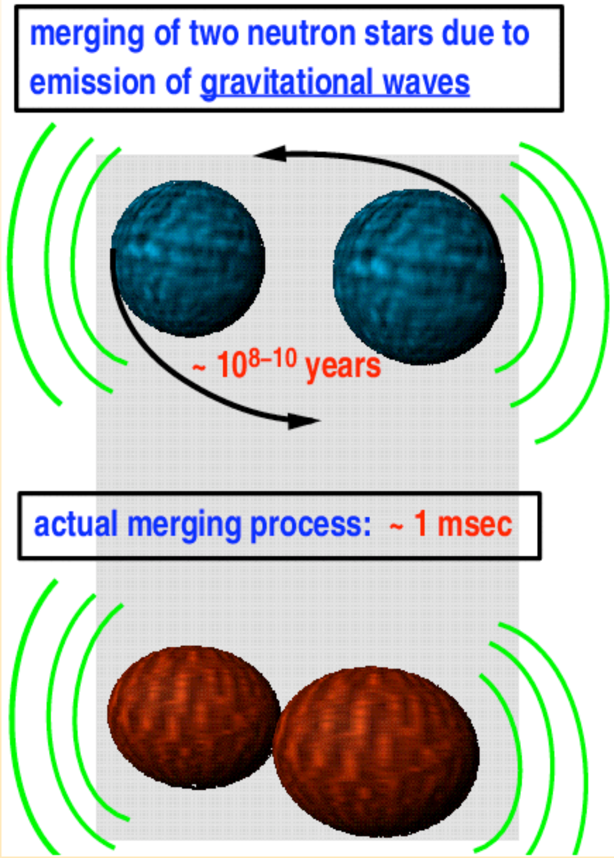

Setting the stage

- The merger of two neutron stars is considered the most promising scenario for the generation of short GRBs.
- After a phase of inspiral due to the loss of angular momentum and orbital energy by gravitational radiation, the merging NSs are distorted by their mutual tidal forces.
- Finally, they touch each other in a contact surface.

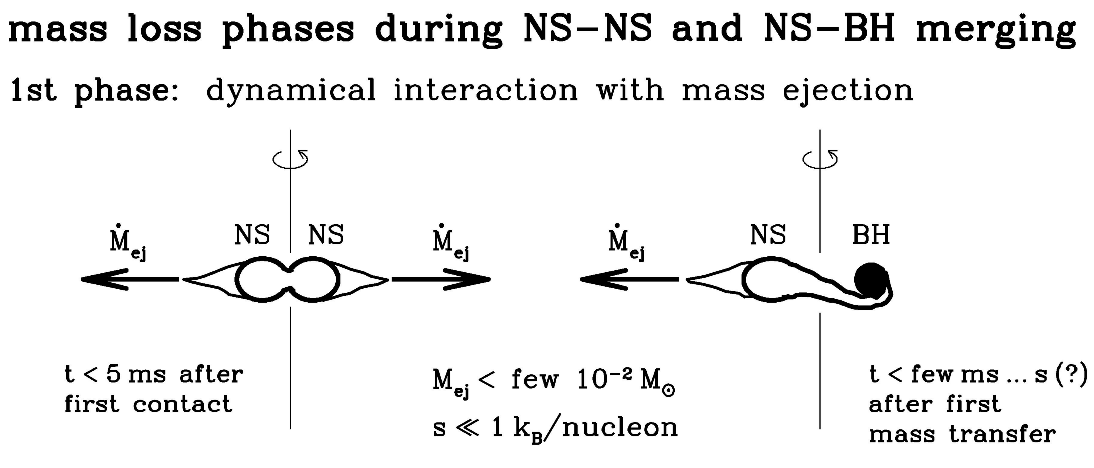

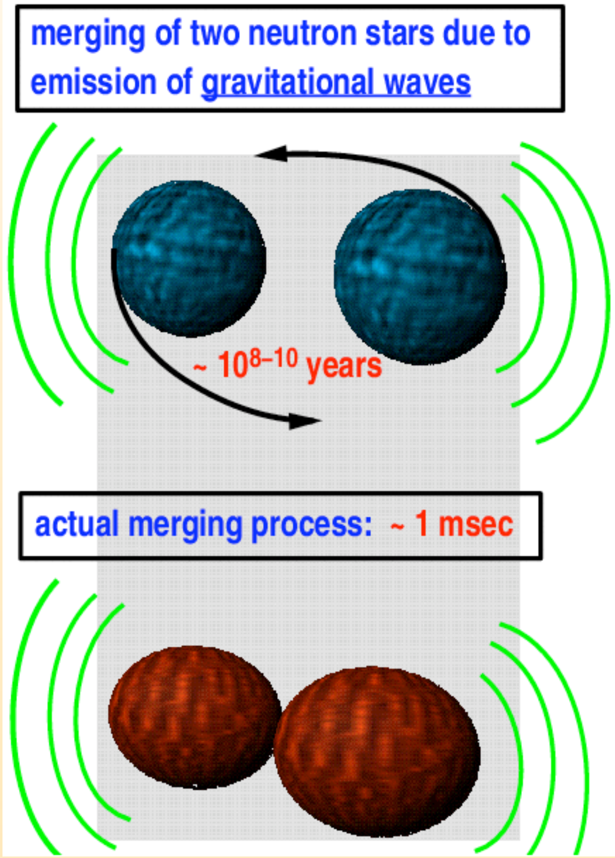

Setting the stage

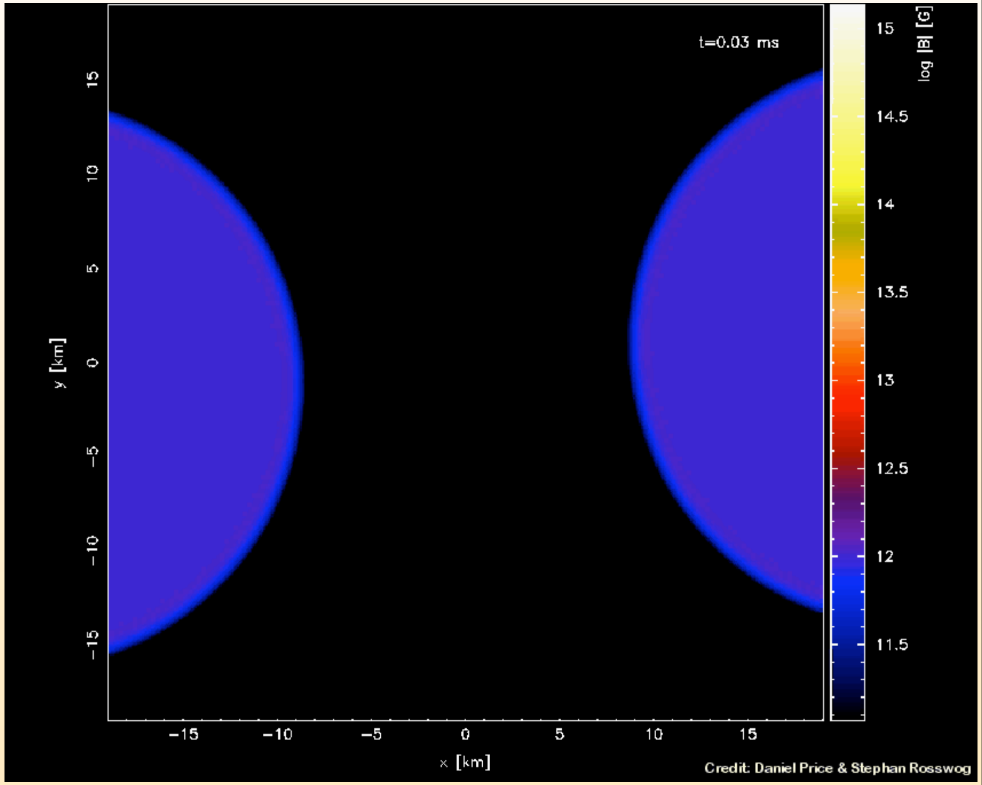

Setting the stage

— Orbital motion + NSs rotation

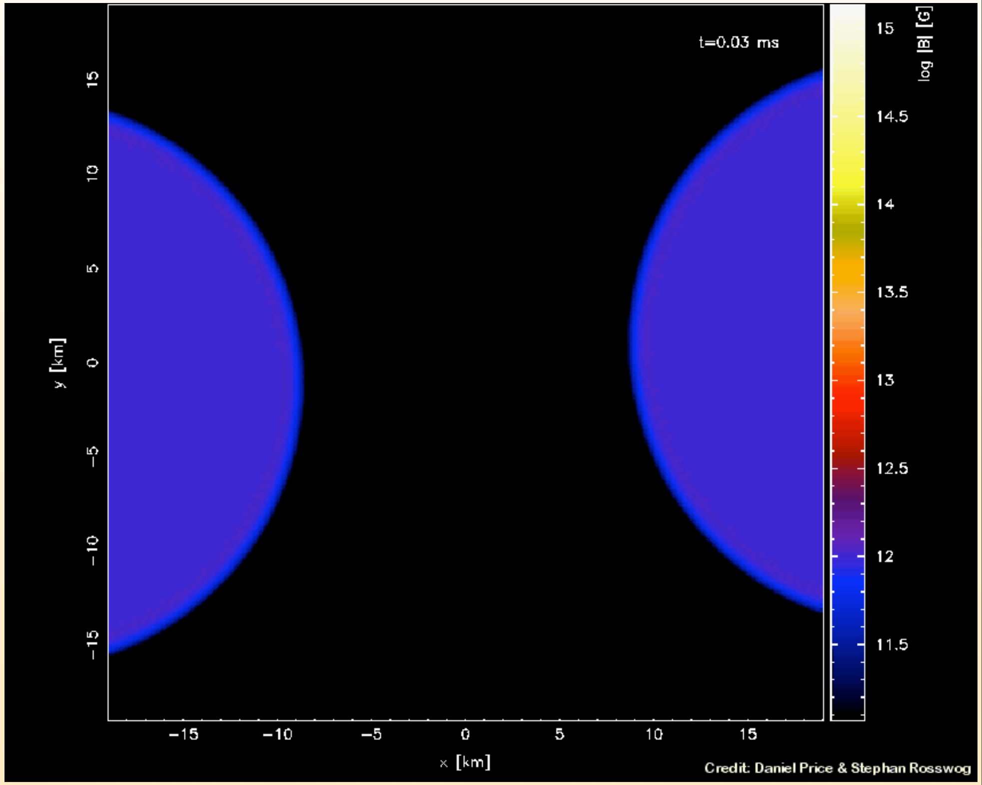

Setting the stage

— Orbital motion + NSs rotation
  ⇒ formation of a KH unstable contact layer.

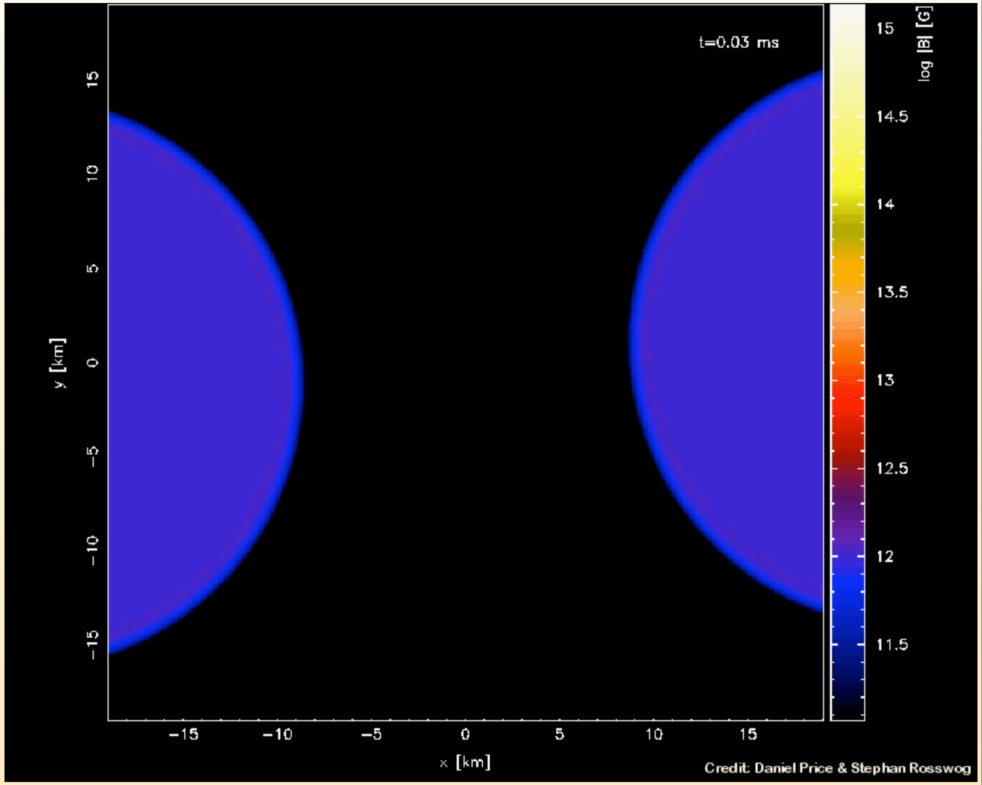

Setting the stage

— Orbital motion + NSs rotation

⇒ formation of a KH unstable contact layer.

— The KH instability leads to the growth (few ms) of KH vortices between the NSs, which can modify the merger dynamics via the dissipation of kinetic into thermal energy (e.g., Oechslin et al. 2007).

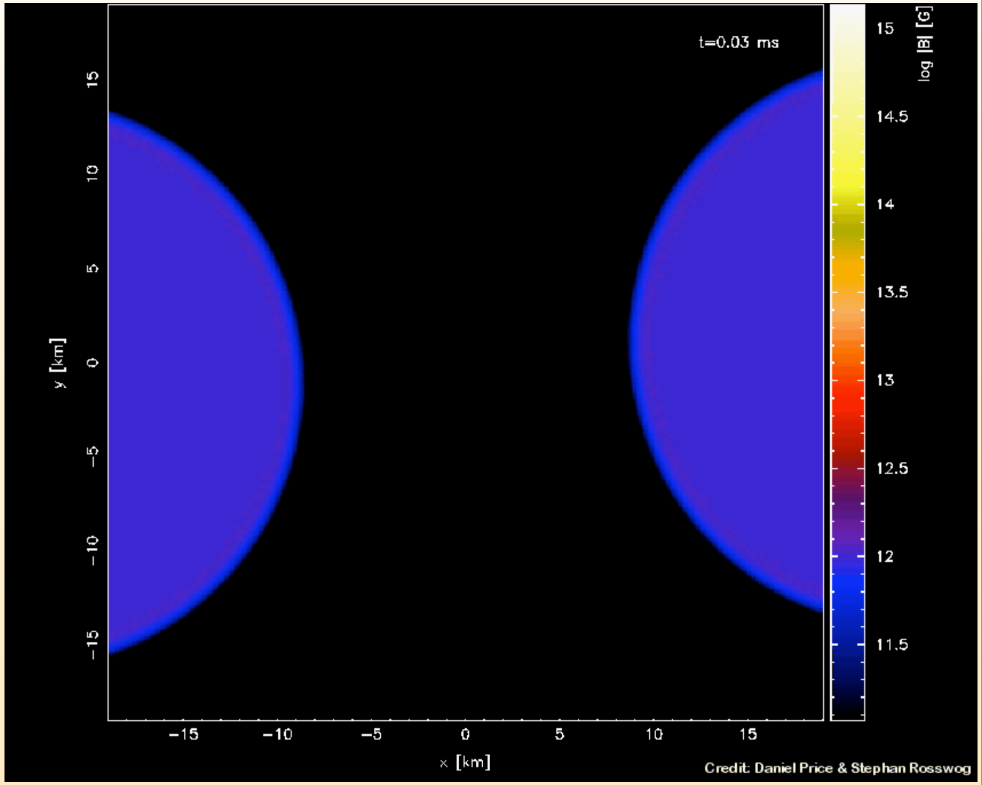

Setting the stage

— Orbital motion + NSs rotation

⇒ formation of a KH unstable contact layer.

— The KH instability leads to the growth (few ms) of KH vortices between the NSs, which can modify the merger dynamics via the dissipation of kinetic into thermal energy (e.g., Oechslin et al. 2007).

— If there is an initial (even small) magnetic field: Exponential amplification can lead to very strong magnetic fields.

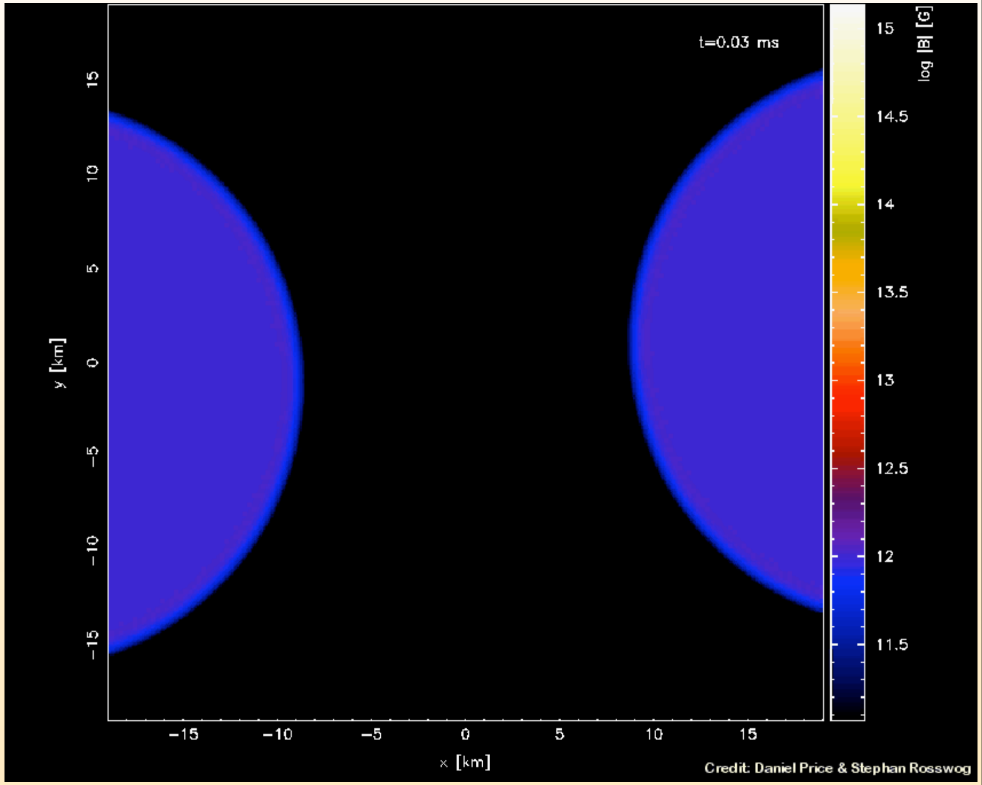

Setting the stage

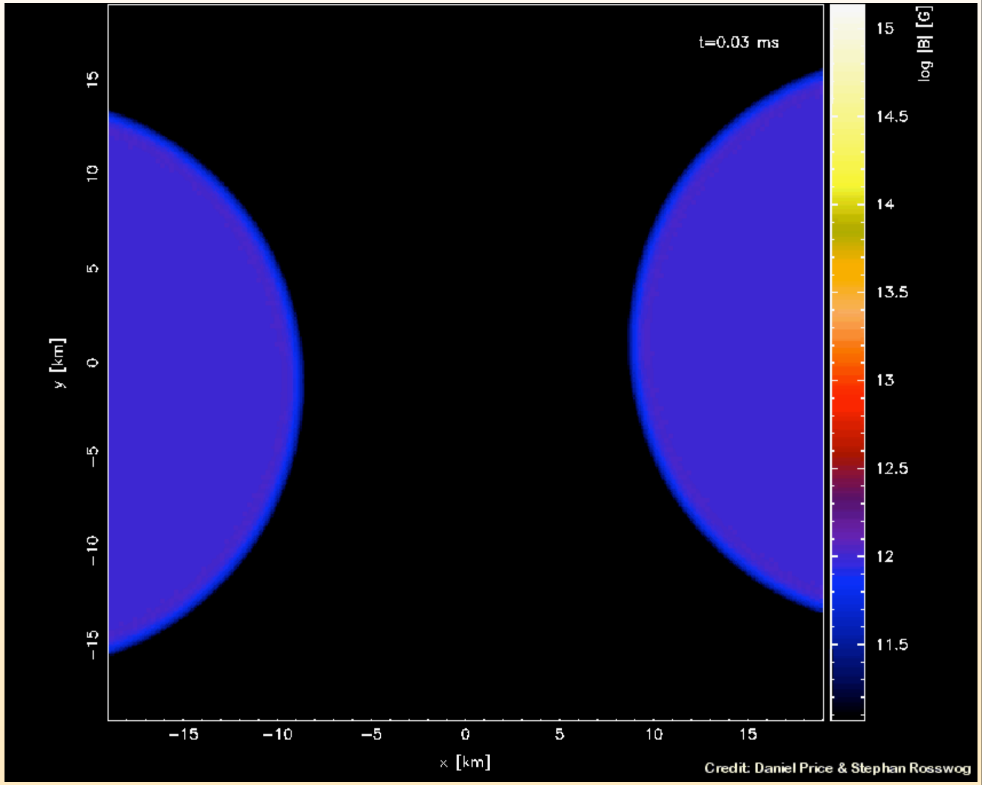

— Orbital motion + NSs rotation

⇒ formation of a KH unstable contact layer.

— The KH instability leads to the growth (few ms) of KH vortices between the NSs, which can modify the merger dynamics via the dissipation of kinetic into thermal energy (e.g., Oechslin et al. 2007).

— If there is an initial (even small) magnetic field: Exponential amplification can lead to very strong magnetic fields.

— These fields, in turn, can modify the dynamics of the instability, either already during the linear growth phase or, for weak fields, in the saturated state.

— $|B|^{max}$: limited by the non-linear dynamics (stresses on the flow or work against fluid forces make e_{mag} to decrease).

Setting the stage

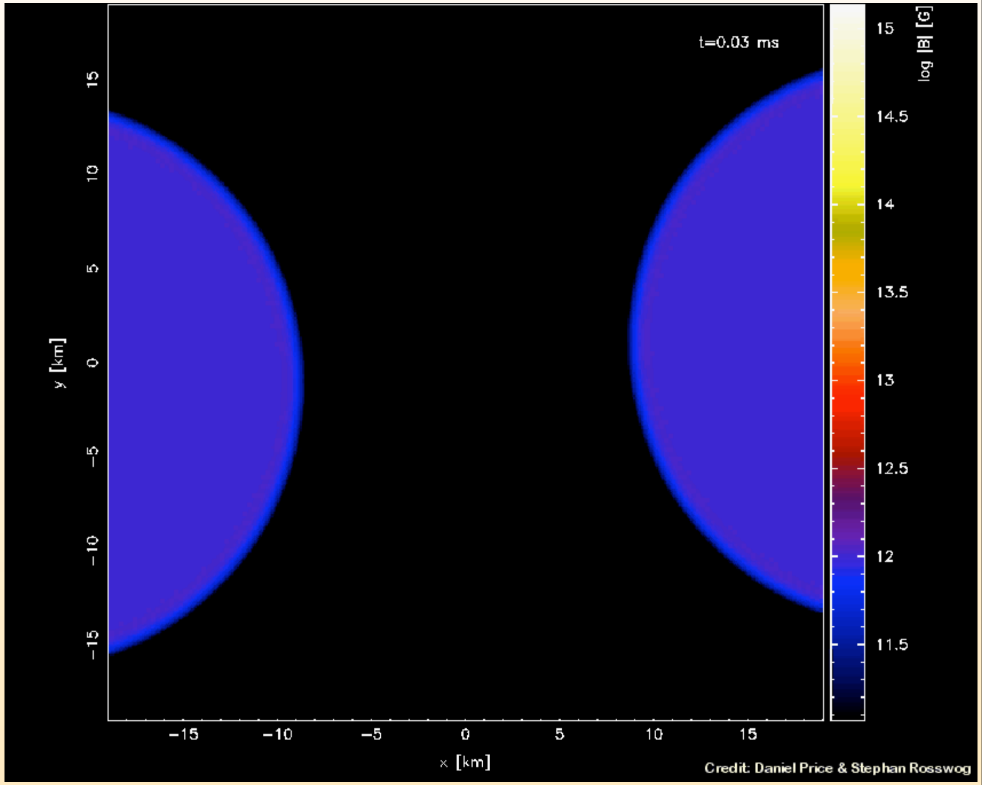

— Orbital motion + NSs rotation

⇒ formation of a KH unstable contact layer.

— The KH instability leads to the growth (few ms) of KH vortices between the NSs, which can modify the merger dynamics via the dissipation of kinetic into thermal energy (e.g., Oechslin et al. 2007).

— If there is an initial (even small) magnetic field: Exponential amplification can lead to very strong magnetic fields.

— These fields, in turn, can modify the dynamics of the instability, either already during the linear growth phase or, for weak fields, in the saturated state.

— $|B|^{max}$: limited by the non-linear dynamics (stresses on the flow or work against fluid forces make e_{mag} to decrease).

— Price & Rosswog (2006); Rosswog (2007) obtain $|B|^{max} > 10^{15}$ G.

Setting the stage

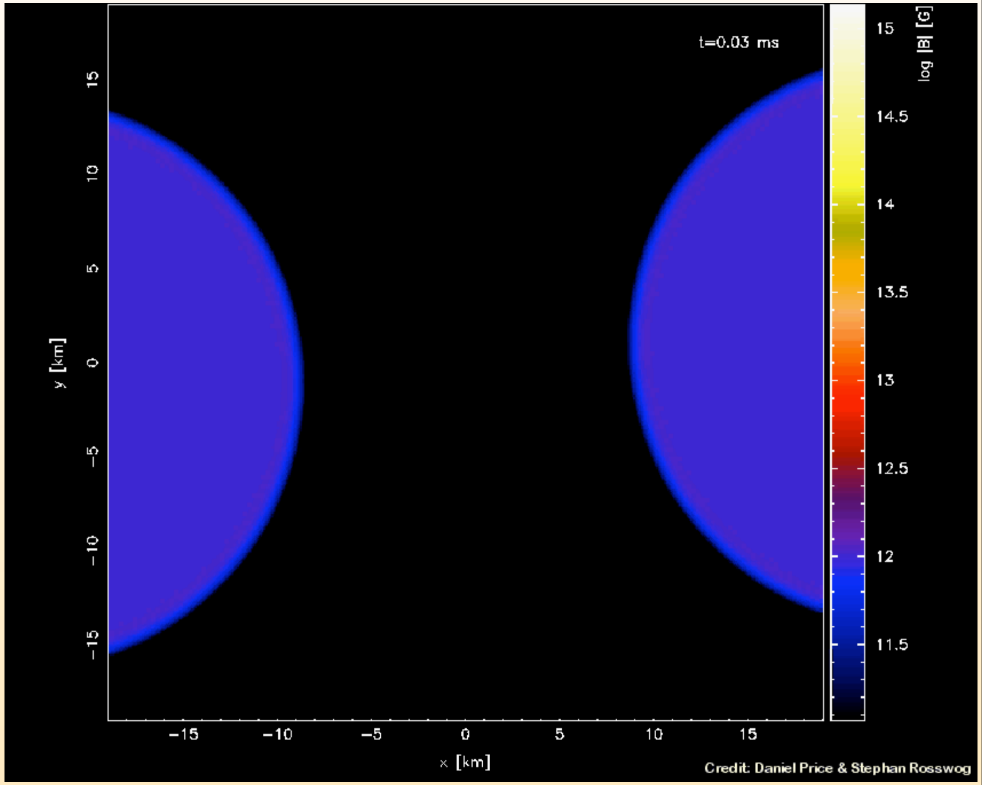

— Orbital motion + NSs rotation

⇒ formation of a KH unstable contact layer.

— The KH instability leads to the growth (few ms) of KH vortices between the NSs, which can modify the merger dynamics via the dissipation of kinetic into thermal energy (e.g., Oechslin et al. 2007).

— If there is an initial (even small) magnetic field: Exponential amplification can lead to very strong magnetic fields.

— These fields, in turn, can modify the dynamics of the instability, either already during the linear growth phase or, for weak fields, in the saturated state.

— $|B|^{max}$: limited by the non-linear dynamics (stresses on the flow or work against fluid forces make e_{mag} to decrease).

— Price & Rosswog (2006); Rosswog (2007) obtain $|B|^{max} > 10^{15}$ G.

— Results handicapped by insufficient numerical resolution, particularly in the non-linear KH phase:

Setting the stage

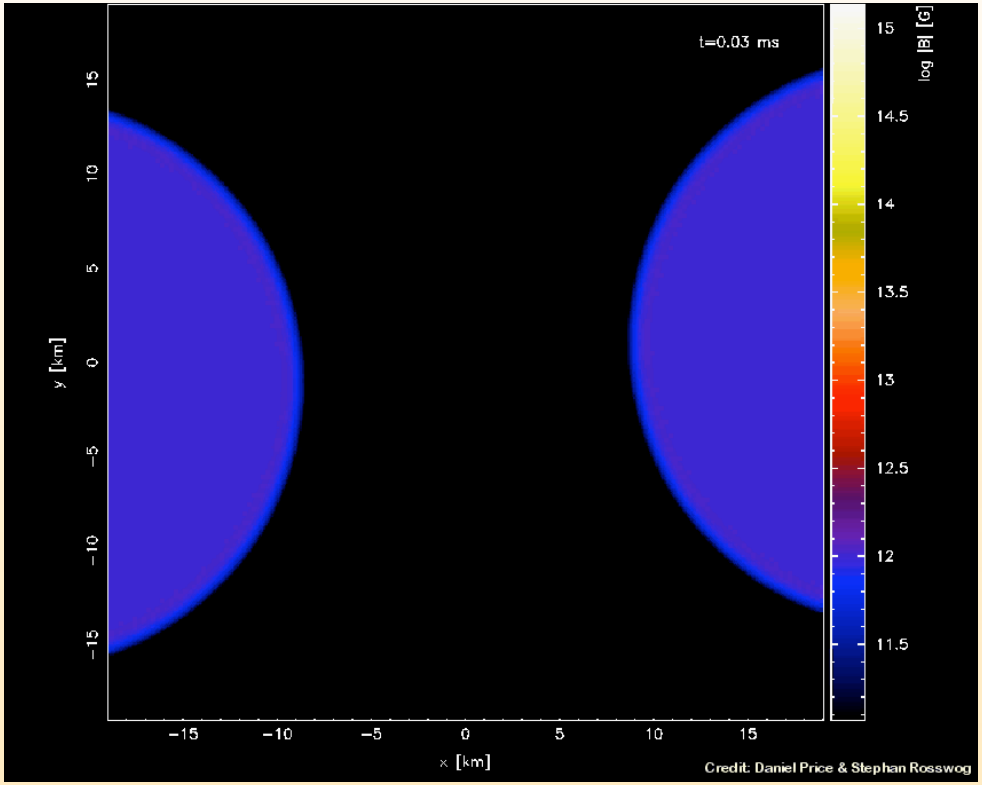

— Orbital motion + NSs rotation

⇒ formation of a KH unstable contact layer.

— The KH instability leads to the growth (few ms) of KH vortices between the NSs, which can modify the merger dynamics via the dissipation of kinetic into thermal energy (e.g., Oechslin et al. 2007).

— If there is an initial (even small) magnetic field: Exponential amplification can lead to very strong magnetic fields.

— These fields, in turn, can modify the dynamics of the instability, either already during the linear growth phase or, for weak fields, in the saturated state.

— $|B|^{max}$: limited by the non-linear dynamics (stresses on the flow or work against fluid forces make e_{mag} to decrease).

— Price & Rosswog (2006); Rosswog (2007) obtain $|B|^{max} > 10^{15}$ G.

— Results handicapped by insufficient numerical resolution, particularly in the non-linear KH phase:

➡ No definite conclusions on the maximum strength of the field nor its back-reaction on the fluid.

Setting the stage

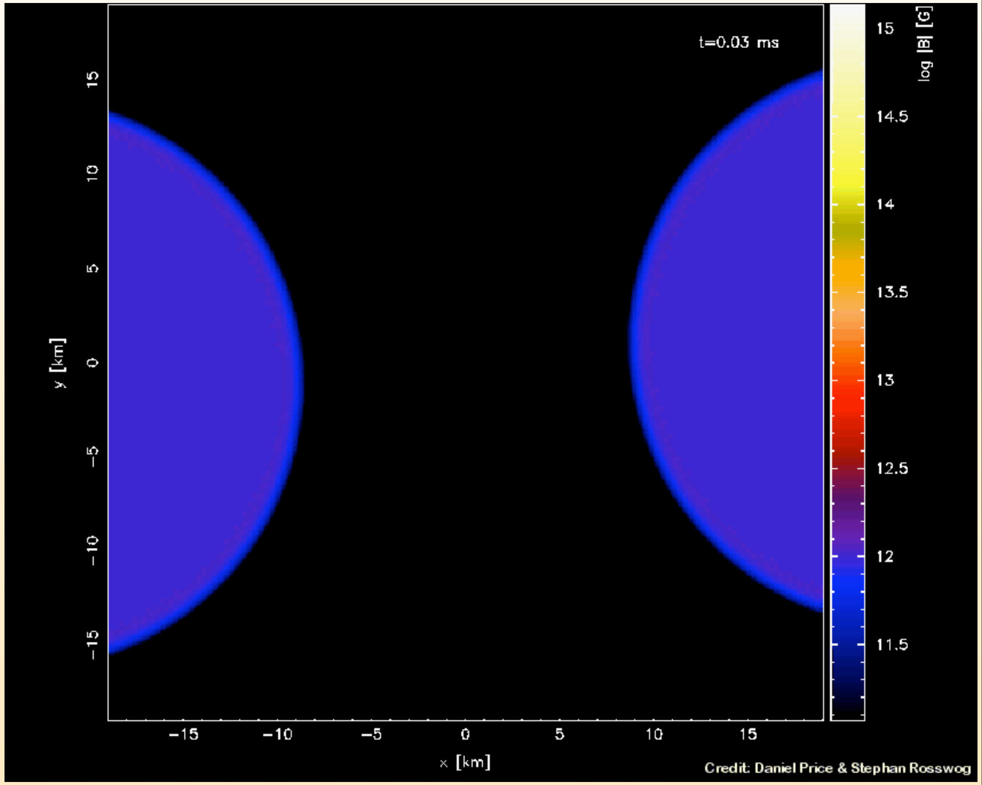

— Orbital motion + NSs rotation

⇒ formation of a KH unstable contact layer.

— The KH instability leads to the growth (few ms) of KH vortices between the NSs, which can modify the merger dynamics via the dissipation of kinetic into thermal energy (e.g., Oechslin et al. 2007).

— If there is an initial (even small) magnetic field: Exponential amplification can lead to very strong magnetic fields.

— These fields, in turn, can modify the dynamics of the instability, either already during the linear growth phase or, for weak fields, in the saturated state.

— $|B|^{max}$: limited by the non-linear dynamics (stresses on the flow or work against fluid forces make e_{mag} to decrease).

— Price & Rosswog (2006); Rosswog (2007) obtain $|B|^{max} > 10^{15}$ G.

— Results handicapped by insufficient numerical resolution, particularly in the non-linear KH phase:

➡ No definite conclusions on the maximum strength of the field nor its back-reaction on the fluid.

➡ The maximum field was a function of the numerical resolution: *the better the resolution, the higher was the field amplification*.

Setting the stage

Setting the stage

➡ Performing numerical convergence tests, these authors could not find an upper bound on $|B|^{max}$. Thus, Price & Rosswog (2006) discussed, based on energetic arguments (no simulation results!), two different saturation levels:

Setting the stage

➡ Performing numerical convergence tests, these authors could not find an upper bound on $|B|^{max}$. Thus, Price & Rosswog (2006) discussed, based on energetic arguments (no simulation results!), two different saturation levels:

- Kinetic equipartition, $e_{mag} \sim e_{kin}$: $|B|^{max} \sim 10^{16}$ G

Setting the stage

➡ Performing numerical convergence tests, these authors could not find an upper bound on $|B|^{max}$. Thus, Price & Rosswog (2006) discussed, based on energetic arguments (no simulation results!), two different saturation levels:

- Kinetic equipartition, $e_{mag} \sim e_{kin}$: $|B|^{max} \sim 10^{16}$ G
- Thermal equipartition, $e_{mag} \sim e_{int}$: $|B|^{max} \sim 10^{18}$ G

Setting the stage

➡ Performing numerical convergence tests, these authors could not find an upper bound on $|B|^{max}$. Thus, Price & Rosswog (2006) discussed, based on energetic arguments (no simulation results!), two different saturation levels:

- Kinetic equipartition, $e_{mag} \sim e_{kin}$: $|B|^{max} \sim 10^{16}$ G
- Thermal equipartition, $e_{mag} \sim e_{int}$: $|B|^{max} \sim 10^{18}$ G

➡ Other groups have addressed a similar problem with different degrees of sophistication in their global numerical simulations (Giacomazzo et al. 2009, Liu et al. 2008, Anderson et al. 2008).

Setting the stage

➡ Performing numerical convergence tests, these authors could not find an upper bound on $|B|^{max}$. Thus, Price & Rosswog (2006) discussed, based on energetic arguments (no simulation results!), two different saturation levels:

- Kinetic equipartition, $e_{mag} \sim e_{kin}$: $|B|^{max} \sim 10^{16}$ G
- Thermal equipartition, $e_{mag} \sim e_{int}$: $|B|^{max} \sim 10^{18}$ G

➡ Other groups have addressed a similar problem with different degrees of sophistication in their global numerical simulations (Giacomazzo et al. 2009, Liu et al. 2008, Anderson et al. 2008).

➡ Our opinion: global numerical simulations do not reach sufficient numerical resolution to study instabilities and turbulence. We need local numerical simulations (LNS):

Setting the stage

- ➡ Performing numerical convergence tests, these authors could not find an upper bound on $|B|^{max}$. Thus, Price & Rosswog (2006) discussed, based on energetic arguments (no simulation results!), two different saturation levels:
  - Kinetic equipartition, $e_{mag} \sim e_{kin}$: $|B|^{max} \sim 10^{16}$ G
  - Thermal equipartition, $e_{mag} \sim e_{int}$: $|B|^{max} \sim 10^{18}$ G
- ➡ Other groups have addressed a similar problem with different degrees of sophistication in their global numerical simulations (Giacomazzo et al. 2009, Liu et al. 2008, Anderson et al. 2008).
- ➡ Our opinion: global numerical simulations do not reach sufficient numerical resolution to study instabilities and turbulence. We need local numerical simulations (LNS):
  - SPH has higher numerical viscosity than to grid based methods (Agertz et al. 2007).

Setting the stage

- ➡ Performing numerical convergence tests, these authors could not find an upper bound on $|B|^{max}$. Thus, Price & Rosswog (2006) discussed, based on energetic arguments (no simulation results!), two different saturation levels:
  - Kinetic equipartition, $e_{mag} \sim e_{kin}$: $|B|^{max} \sim 10^{16}$ G
  - Thermal equipartition, $e_{mag} \sim e_{int}$: $|B|^{max} \sim 10^{18}$ G
- ➡ Other groups have addressed a similar problem with different degrees of sophistication in their global numerical simulations (Giacomazzo et al. 2009, Liu et al. 2008, Anderson et al. 2008).
- ➡ Our opinion: global numerical simulations do not reach sufficient numerical resolution to study instabilities and turbulence. We need local numerical simulations (LNS):
  - SPH has higher numerical viscosity than to grid based methods (Agertz et al. 2007).
  - The best resolution using vertex-centered mesh refinement in global models is h ~350 m (Giacomazzo et al. 2009).

Setting the stage

➡ Performing numerical convergence tests, these authors could not find an upper bound on $|B|^{max}$. Thus, Price & Rosswog (2006) discussed, based on energetic arguments (no simulation results!), two different saturation levels:

- Kinetic equipartition, $e_{mag} \sim e_{kin}$: $|B|^{max} \sim 10^{16}$ G
- Thermal equipartition, $e_{mag} \sim e_{int}$: $|B|^{max} \sim 10^{18}$ G

➡ Other groups have addressed a similar problem with different degrees of sophistication in their global numerical simulations (Giacomazzo et al. 2009, Liu et al. 2008, Anderson et al. 2008).

➡ Our opinion: global numerical simulations do not reach sufficient numerical resolution to study instabilities and turbulence. We need local numerical simulations (LNS):

- SPH has higher numerical viscosity than to grid based methods (Agertz et al. 2007).
- The best resolution using vertex-centered mesh refinement in global models is h ~350 m (Giacomazzo et al. 2009).
- We show that h ~ 0.1 m (in 2D) or h ~ 0.8 m (3D) needed for converged results in LNS.

Goals and methods

Goals and methods

➡ Better understanding of MHD-KH instability:

Goals and methods

- ➡ Better understanding of MHD-KH instability:
  - Influence of the numerical systematics: resolution, boundaries, etc.

Goals and methods

➡ Better understanding of MHD-KH instability:

- Influence of the numerical systematics: resolution, boundaries, etc.
- Generic properties of the saturation of the instability

Goals and methods

➡ Better understanding of MHD-KH instability:

- Influence of the numerical systematics: resolution, boundaries, etc.
- Generic properties of the saturation of the instability

➡ Asses the results of Price & Rosswog:

Goals and methods

➡ Better understanding of MHD-KH instability:

- Influence of the numerical systematics: resolution, boundaries, etc.
- Generic properties of the saturation of the instability

➡ Asses the results of Price & Rosswog:

- $|B|^{max}$ and field topology.

Goals and methods

- ➡ Better understanding of MHD-KH instability:
  - Influence of the numerical systematics: resolution, boundaries, etc.
  - Generic properties of the saturation of the instability
- ➡ Asses the results of Price & Rosswog:
  - $|B|^{max}$ and field topology.
  - growth times of the KHI

Goals and methods

- ➡ Better understanding of MHD-KH instability:
  - Influence of the numerical systematics: resolution, boundaries, etc.
  - Generic properties of the saturation of the instability
- ➡ Asses the results of Price & Rosswog:
  - $|B|^{max}$ and field topology.
  - growth times of the KHI
  - saturation mechanism.

Goals and methods

- ➡ Better understanding of MHD-KH instability:
  - Influence of the numerical systematics: resolution, boundaries, etc.
  - Generic properties of the saturation of the instability
- ➡ Asses the results of Price & Rosswog:
  - $|B|^{max}$ and field topology.
  - growth times of the KHI
  - saturation mechanism.
  - dynamics of supersonic shear flows.
- ➡ Dimensionless/scale-free LNS

Goals and methods

- ➡ Better understanding of MHD-KH instability:
  - Influence of the numerical systematics: resolution, boundaries, etc.
  - Generic properties of the saturation of the instability
- ➡ Asses the results of Price & Rosswog:
  - $|B|^{max}$ and field topology.
  - growth times of the KHI
  - saturation mechanism.
  - dynamics of supersonic shear flows.
- ➡ Dimensionless/scale-free LNS
- ➡ Merger-oriented LNS, where the initial set up mimics merger conditions (density, velocity, magnetic field, etc.)

Goals and methods

➡ Better understanding of MHD-KH instability:

- Influence of the numerical systematics: resolution, boundaries, etc.
- Generic properties of the saturation of the instability

➡ Asses the results of Price & Rosswog:

- $|B|^{max}$ and field topology.
- growth times of the KHI
- saturation mechanism.
- dynamics of supersonic shear flows.

➡ Dimensionless/scale-free LNS

➡ Merger-oriented LNS, where the initial set up mimics merger conditions (density, velocity, magnetic field, etc.)

➡ New (Newtonian) MHD code specifically designed for the study of instabilities and turbulent systems.

The new MHD code in a nutshell

1. Flux-conservative, finite-volume, Eulerian formulation of the ideal MHD equations
2. High-resolution shock capturing methods:
   - various optional high-order reconstruction algorithms:
     - 2nd-order total-variation diminishing piecewise-linear (TVD-PL) scheme (using as slope limiters, Minmod, van Leer or MC).
     - 4th-order weighted essentially non-oscillatory (WENO4) scheme (Levy et al. 2002).
     - 5th-, 7th- and 9th-order monotonicity-preserving (MP5, MP7, MP9) schemes (Suresh & Huynh 1997)
   - Approximate Riemann solvers based on the multi-stage (MUSTA) method (Toro & Titarev 2006).
3. Self-gravity: Poisson solver.
4. Constraint-transport scheme to maintain a $\nabla \mathbf{B} = 0$ (Evans & Hawley 1988):
   - volume averaged hydro quantities, surface averaged B-fields, corner averaged E-fields.
   - Due to the staggering of different variables, careful (high-order) interpolation between different numerical grids.
   - We compute **E** from the velocity and the B-field at cell interface which we get as the result of the Riemann solver: E-field consistent with the solution of the Riemann problem!.
5. Parallel (MPI/OpenMP)-Fortran90 code.

The magnetized KH instability

- The KHI leads to exponential growth of perturbations in a non-magnetised shear layer (SL) of a fluid of background density ρ (e.g., Chandrasekhar 1961).
- If a plane-parallel SL extends over a thickness *d*, all modes with wavelengths $\lambda > d$ are unstable, and the shorter modes grow faster.
- After a phase of exponential growth, a stable KH vortex forms.
- Assume: shear flow in the x-direction,

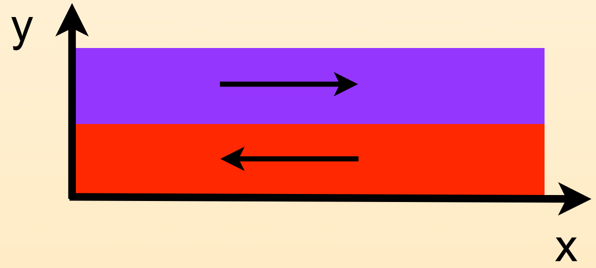

  U_0 = velocity difference across the SL

  $c_A = (b^2 / \rho)^{1/2}$ = Alfvén velocity

  $A = U_0 / c_A$ = Alfvén number

  $b = |b_x|$ = Magnetic field strength (parallel to the SL)

  ✳ A magnetic field perpendicular to the SL and to the shearing interface (b_y field) will be converted into a b_x field by the shear; thus, it leads to a similar dynamics.

  ✳ A field orthogonal to the shear flow but parallel to the interface acts mainly by adding P_{mag} to P_{th}, thus modifying the dynamics of the KHI only to a small degree.

- For strong fields, **A > 2**: stable, no KH growth.
- For weaker fields, **A < 2**: the instability develops similarly to the non-magnetic case, but its growth and its non-linear saturated state may be affected significantly (e.g., Frank et al. 1996; Jones et al. 1997; Jeong et al. 2000; Ryu et al. 2000).

The magnetized KH instability

Summary of previous results for *weak* fields (2D):

- Rather *strong* fields, **A** $\gtrsim$**2**: ***non-linear stabilisation***.
  - Too weak for stabilisation initially, the field is amplified, and, after less than one turnover of the KH vortex, is strong enough to suppress further winding.
  - The field, concentrated in thin sheets, annihilates in localized reconnection and, mediating the conversion $e_{kin} \to e_{mag} \to e_{int}$, destroys the vortex.
  - Late evolution: broad transition layer. The flow is almost parallel to the initial SL. No vortex retained. Reconnection $\to$ strong decrease of *b*, which concentrates in sheet-like patterns.
- Weaker fields: ***disruptive dynamics***.
  - Longer amplification times $\Longrightarrow$ the vortex retains its coherence over more cicles.
  - During this process, the field is wound up in increasingly thin sheets, which, eventually, will reconnect due to (numerical) resistivity.
  - Late evolution: similar to the previous case. the vortex is disrupted, leading to a broad laminar transition region threaded by filamentary magnetic fields.
- Even weaker fields: ***dissipative dynamics***.
  - After a long phase of amplification $\Longrightarrow$ insufficient field growth to affect the flow.
  - Reconnection occurs, but, due to the weak fields involved: gradual conversion $e_{kin} \to e_{int}$.
  - Late evolution: The vortex remains coherent, with decreasing velocity as e_{kin} is extracted.
- Transition between regimes: no clear separation in A.

In 3D, even **HD instabilities** can disrupt the vortex. MHD instabilities add on top of the HD effects (Ryu et al. 2000).

Numerical setup

$b(t=0) = (\, b_x{}^0, 0, 0)$

Ideal gas EoS:
P = $(\gamma$-1$)\,\rho\varepsilon$

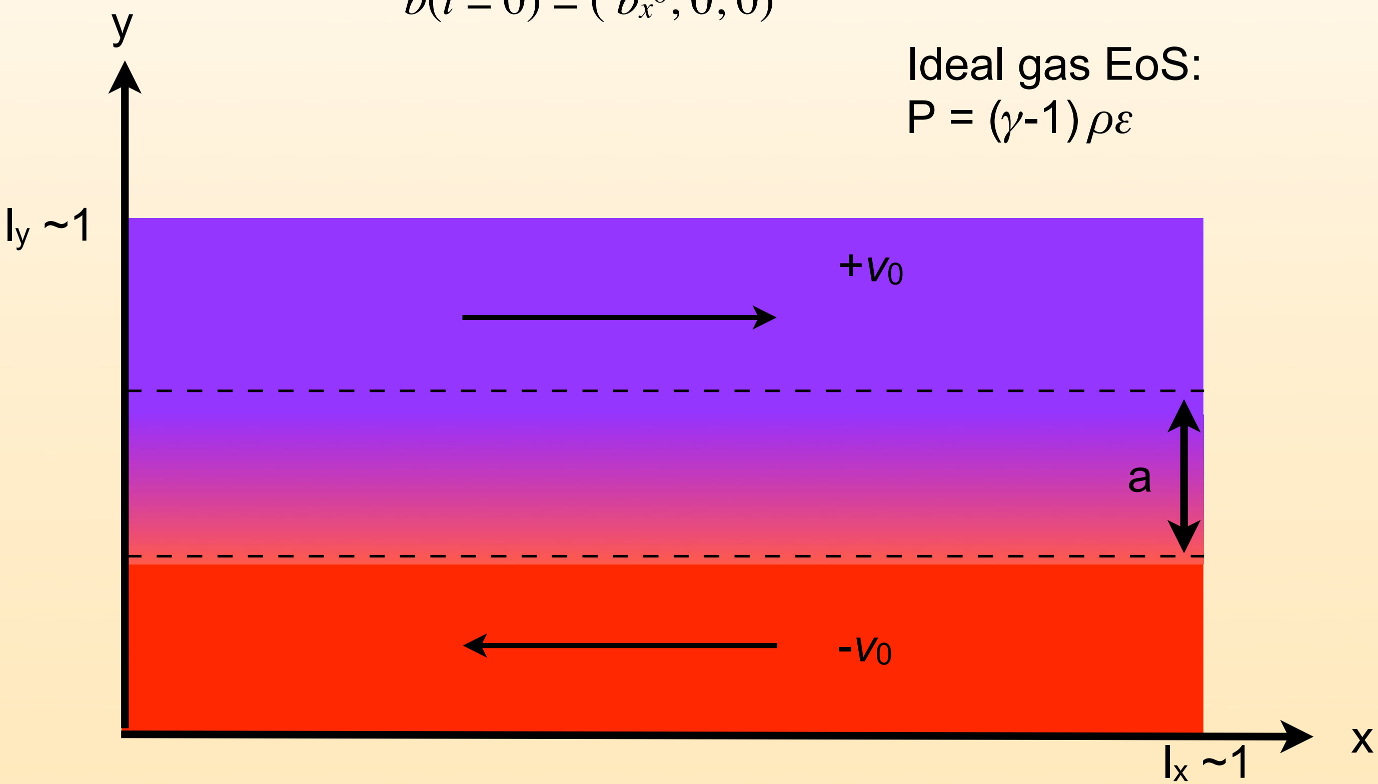

$$\left(v_x, v_y, v_z\right)^T = \left(v_0 \tanh\frac{y}{a}, 0, 0\right)^T$$

$$U_0 = 2v_0$$

$v_y(t=0) = v_y^0 f(y)\sin(k_x x)$ instability trigger

$v_y{}^0$~ 10^{-8} - $10^{-6} v_0$

$f(y) \in [0, 1]$ vanishes at $|y|=4a$

Numerical validation: linear growth

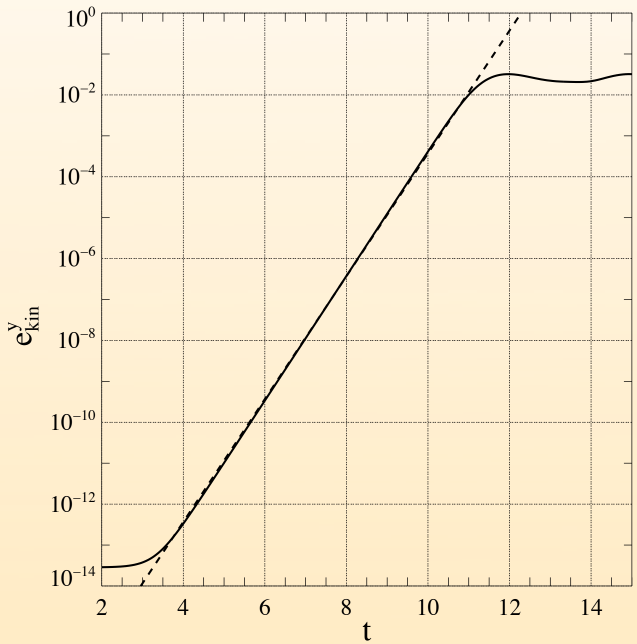

We capture the analytic linear growth in all models $\Longrightarrow$ the code works fine!

We use the same models as Keppens et al. (1999) and Miura & Pritchett (1982), from where we take Γ_{MP}.

SUBSONIC REGIME

	name	l_x	l_y	$m_x \times m_y$	P_0	U_0	M	a	$\boldsymbol{b}_0$	k_x	Γ_{MP}	Γ_{num}
HD models	grw-1	1	2	50×100	1	1.29	1	0.05	$(0,0,0)$	2π	1.73	1.64
	grw-2	1	2	100×200	1	1.29	1	0.05	$(0,0,0)$	2π	1.73	1.74
	grw-3	1	2	200×400	1	1.29	1	0.05	$(0,0,0)$	2π	1.73	1.75
	grw-4	1	2	400×800	1	1.29	1	0.05	$(0,0,0)$	2π	1.73	1.75
	grw-5	1	2	200×400	1	1.29	1	0.025	$(0,0,0)$	2π	2.4	2.44
	grw-6	1	2	200×400	1	1.29	1	0.1	$(0,0,0)$	2π	0.66	0.68
	grw-7	1	2	200×400	1	0.645	0.5	0.05	$(0,0,0)$	2π	1.09	1.07
	grw-8	1	2	200×400	1	1.843	10/7	0.05	$(0,0,0)$	2π	1.77	1.79
	grw-9	1	2	200×400	1	0.645	0.5	0.05	$(0,0,0)$	4π	1.36	1.35
MHD models	grw-10	1	2	200×400	1	1.29	1	0.05	$(0.129,0,0)$	2π	1.69	1.70
	grw-11	1	2	200×400	1	1.29	1	0.05	$(0.258,0,0)$	2π	1.56	1.54

Influence of BCs and domain size

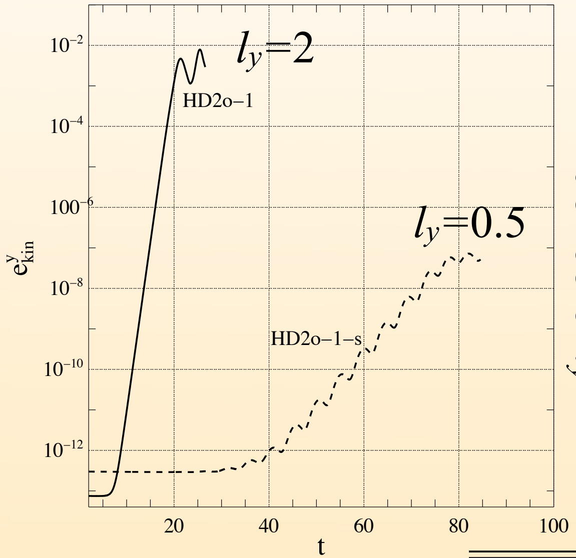

Influence of l_y

- We test domain size and BC influence with supersonic models (M>1).
- Miura & Pritchett (1982): **No growth if M ≥ 2**
- Smaller domains (with the same resolution *h* per dimension!) bring oscillatory growth, with damping of Γ_{num}.
- Open boundaries yield larger Γ_{num} if l_y is sufficiently large, otherwise opposite effect.

SUPERSONIC (HD) REGIME

name	l_x	l_y	$m_x \times m_y$	P_0	U_0	M	a	k_x	BC	Γ_{num}	oscillations
HD2o-1-l	1	4	200 × 800	1	2.322	1.8	0.05	2π	open	0.97	
HD2o-1	1	2	200 × 400	1	2.322	1.8	0.05	2π	open	0.96	
HD2o-1-i	1	1	200 × 200	1	2.322	1.8	0.05	2π	open	0.73	
HD2o-1-s	1	0.5	200 × 100	1	2.322	1.8	0.05	2π	open	0.16	√
HD2o-2	1	2	200 × 400	1	2.451	1.9	0.05	2π	open	0.30	√
HD2o-3	1	2	200 × 400	1	2.5155	1.95	0.05	2π	open	0.26	√
HD2o-4	1	2	200 × 400	1	2.58	2	0.05	2π	open	0	
HD2o-5	1	2	200 × 400	1	5.16	4	0.05	2π	open	0	
HD2r-0	1	2	200 × 400	1	1.29	1	0.05	2π	reflecting	1.73	
HD2r-1	1	2	200 × 400	1	2.322	1.8	0.05	2π	reflecting	0.96	
HD2r-1-i	1	1	200 × 200	1	2.322	1.8	0.05	2π	reflecting	0.56	
HD2r-1-s	1	0.5	200 × 100	1	2.322	1.8	0.05	2π	reflecting	0.56	√
HD2r-1-S	1	0.25	200 × 50	1	2.322	1.8	0.05	2π	reflecting	0.35	√
HD2r-4	1	2	200 × 400	1	2.58	2	0.05	2π	reflecting	0.46	√
HD2r-4-HR	1	2	400 × 800	1	2.58	2	0.05	2π	reflecting	0.44	√
HD2r-5	1	2	200 × 400	1	5.16	4	0.05	2π	reflecting	0.52	√

Influence of BCs and domain size

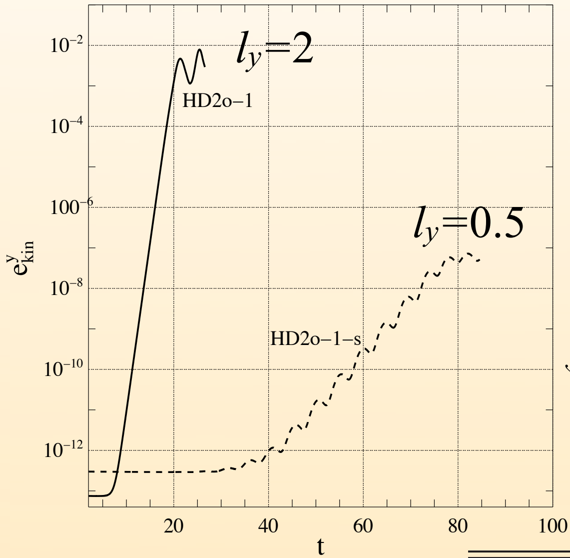

Influence of l_y

- The instability affects a larger area if l_y is sufficiently large.
- sound waves created at the SL steepen into shocks ***if*** they can travel away for a ***sufficiently long distance***.
- Sound/shock waves leaving the domain responsible for the oscillatory growth.
- Only if shocks form $\Longrightarrow$ a vortex-like structure.
- **The y-distance shocks travel depends on M.**
  - For M=1, shocks are restricted to -0.25<y<0.25 $\Longrightarrow$ explains the lack of influence of the BCs.

SUPERSONIC (HD) REGIME

name	l_x	l_y	$m_x \times m_y$	P_0	U_0	M	a	k_x	BC	$\Gamma_{\rm num}$	oscillations
HD2o-1-l	1	4	200 × 800	1	2.322	1.8	0.05	2π	open	0.97	
HD2o-1	1	2	200 × 400	1	2.322	1.8	0.05	2π	open	0.96	
HD2o-1-i	1	1	200 × 200	1	2.322	1.8	0.05	2π	open	0.73	
HD2o-1-s	1	0.5	200 × 100	1	2.322	1.8	0.05	2π	open	0.16	√
HD2o-2	1	2	200 × 400	1	2.451	1.9	0.05	2π	open	0.30	√
HD2o-3	1	2	200 × 400	1	2.5155	1.95	0.05	2π	open	0.26	√
HD2o-4	1	2	200 × 400	1	2.58	2	0.05	2π	open	0	
HD2o-5	1	2	200 × 400	1	5.16	4	0.05	2π	open	0	
HD2r-0	1	2	200 × 400	1	1.29	1	0.05	2π	reflecting	1.73	
HD2r-1	1	2	200 × 400	1	2.322	1.8	0.05	2π	reflecting	0.96	
HD2r-1-i	1	1	200 × 200	1	2.322	1.8	0.05	2π	reflecting	0.56	
HD2r-1-s	1	0.5	200 × 100	1	2.322	1.8	0.05	2π	reflecting	0.56	√
HD2r-1-S	1	0.25	200 × 50	1	2.322	1.8	0.05	2π	reflecting	0.35	√
HD2r-4	1	2	200 × 400	1	2.58	2	0.05	2π	reflecting	0.46	√
HD2r-4-HR	1	2	400 × 800	1	2.58	2	0.05	2π	reflecting	0.44	√
HD2r-5	1	2	200 × 400	1	5.16	4	0.05	2π	reflecting	0.52	√

Growth in the supersonic regime

- Miura & Pritchett (1982): No growth if M ≥ 2.
- We find also (oscillatory) growth if reflecting BC are imposed for M>2.
  $\Longrightarrow \Gamma_{\text{num}}$ almost unchanged if resolution increases.
- Very fast growth happens if M≳1
- If shocks develop, the fluid tries to slide parallel to them in the y-direction. This process mediates a very efficient conversion of e_{kin}^x into e_{kin}^y.

SUPERSONIC (HD) REGIME

name	l_x	l_y	$m_x \times m_y$	P_0	U_0	M	a	k_x	BC	Γ_{num}	oscillations
HD2o-1-l	1	4	200×800	1	2.322	1.8	0.05	2π	open	0.97	
HD2o-1	1	2	200×400	1	2.322	1.8	0.05	2π	open	0.96	
HD2o-1-i	1	1	200×200	1	2.322	1.8	0.05	2π	open	0.73	
HD2o-1-s	1	0.5	200×100	1	2.322	1.8	0.05	2π	open	0.16	√
HD2o-2	1	2	200×400	1	2.451	1.9	0.05	2π	open	0.30	√
HD2o-3	1	2	200×400	1	2.5155	1.95	0.05	2π	open	0.26	√
HD2o-4	1	2	200×400	1	2.58	2	0.05	2π	open	0	
HD2o-5	1	2	200×400	1	5.16	4	0.05	2π	open	0	
HD2r-0	1	2	200×400	1	1.29	1	0.05	2π	reflecting	1.73	
HD2r-1	1	2	200×400	1	2.322	1.8	0.05	2π	reflecting	0.96	
HD2r-1-i	1	1	200×200	1	2.322	1.8	0.05	2π	reflecting	0.56	
HD2r-1-s	1	0.5	200×100	1	2.322	1.8	0.05	2π	reflecting	0.56	√
HD2r-1-S	1	0.25	200×50	1	2.322	1.8	0.05	2π	reflecting	0.35	√
HD2r-4	1	2	200×400	1	2.58	2	0.05	2π	reflecting	0.46	√
HD2r-4-HR	1	2	400×800	1	2.58	2	0.05	2π	reflecting	0.44	√
HD2r-5	1	2	200×400	1	5.16	4	0.05	2π	reflecting	0.52	√

Magnetized models: non-linear stabilization for intermediate fields

- Our standard setup: l_x x l_y = 2 x 2; reflecting BCs; U_0=1; M=1, 4; γ=4/3

- Strong fields: we verify the linear stability results, which imply stabilization for A≤2.

- Weaker fields: we run models with A>2, finding excellent agreement with Frank et al. (1996), e.g.:

  - non-linear stabilization for, e.g., A=2.5
  - for A=5 $\Longrightarrow$ the KH vortex can form and winds up the B-field, which eventually becomes strong enough $\Longrightarrow$ non-linear stabilization.

➡ The B-field stabilizes the growth of KH modes, either linearly or non-linearly if A≲5.

Magnetized models: non-linear stabilization for intermediate fields

- Notes on numerical resistivity:
  - For $R_{em} \to \infty \Longrightarrow$ energy is transferred to ever smaller scales in turbulent cascades.
  - In numerical simulations, eventually the energy reaches the grid scale, *h*, where it cannot be represented by the discretized B-fields. Thus, it is assigned to e_{int}.
  - Physical resistivity transfers also $e_{mag} \to e_{int}$, hence, *numerical resistivity acts as a subgrid model for unresolved dynamics*.
- In models with **intermediate fields, $2 \lesssim A \lesssim 5$**, due to numerical resistivity, the emergence of coherent flow and field structures is subsequently disrupted in reconnection events $\Longrightarrow$ efficient conversion $e_{kin} \to e_{mag} \to e_{int}$, much more efficient than $e_{kin} \to e_{int}$ in HD-models.
- Final flow: rather laminar than turbulent, with broad SL (agreement with Jones et al. 1997).

Magnetized models: weak fields (reproducing previous results)

- Prototype models with A=125 and A=5000, computed with resolutions up to 4096^2.
- We identify the same disruption and dissipation regimes as Jones et al. (1997).
- Disruption regime:
  - B-field wound up in very thin sheets. If the sheets approach each other (having opposite polarity) reconnection happens
    $\Longrightarrow$ tearing- mode instability.
  - Tearing modes behave as catalyst $e_{kin} \longrightarrow e_{int}$ conversion.
- Dissipation regime:
  - Same effects as in the disruption regime + growth of the B-field to values such that the flows produced in tearing modes can disrupt the KH-vortex.
  - Final state: turbulent layer where the flow and field decay slowly until $e_{kin}^{y} \longrightarrow e_{mag}^{y}$.

Magnetized models: weak fields (new results)

The evolution of weakly magnetized models can be separated in three phases:

1. **KH-phase** (as predicted by the linear theory).
2. **Kinematic phase** (B-amplification after formation of the vortex which evolves secularly).
3. **Dissipation/disruption phase** (the KH vortex looses its energy by magnetic stresses).

Magnetized models: weak fields KH-phase

- Our models grow with $\Gamma_{num}^{MHD} \sim \Gamma_{num}^{HD}$.
- Passive field amplification.
- Fixed amplification factor by the end of this phase (model independent):

$$|B|_{KH} \sim 1.4\ |B_0|$$

- By the end of the KH-phase:

$$e_{mag}^{y} \sim 0.1 \times e_{mag}$$

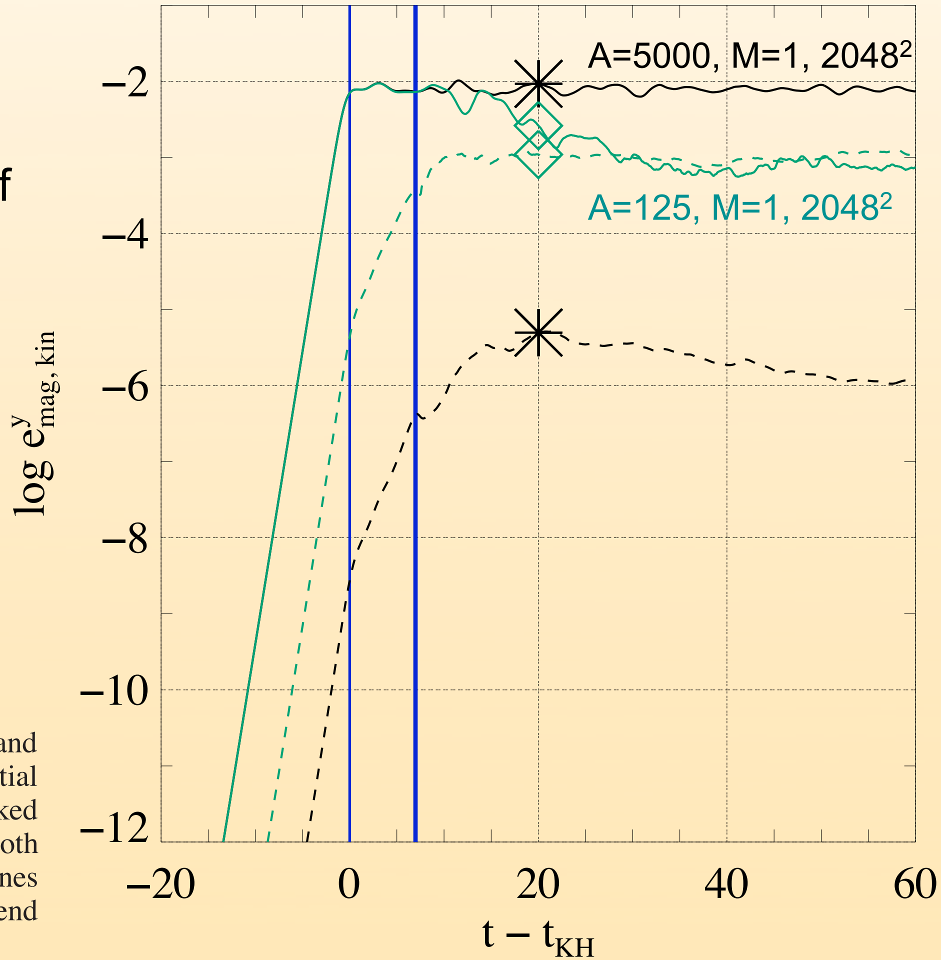

Fig. 3. The temporal evolution of the transverse kinetic (solid lines) and magnetic (dashed lines) energies per unit volume for models with initial Mach and Alfvén numbers of M = 1 and A = 125 (green lines, marked by a diamond) and A = 5000 (black lines, marked by an asterisk). Both models were computed on a grid of 2048^2 zones. The blue vertical lines indicate the end of the KH phase, t_{KH}, and an approximation of the end of the kinematic phase.

Magnetized models: weak fields KH-phase

- Our models grow with $\Gamma_{num}^{MHD} \sim \Gamma_{num}^{HD}$.
- Passive field amplification.
- Fixed amplification factor by the end of this phase (model independent):

$$|B|_{KH} \sim 1.4\ |B_0|$$

- By the end of the KH-phase:

$$e_{mag}^{y} \sim 0.1 \times e_{mag}$$

- Γ_{num} independent of resolution.

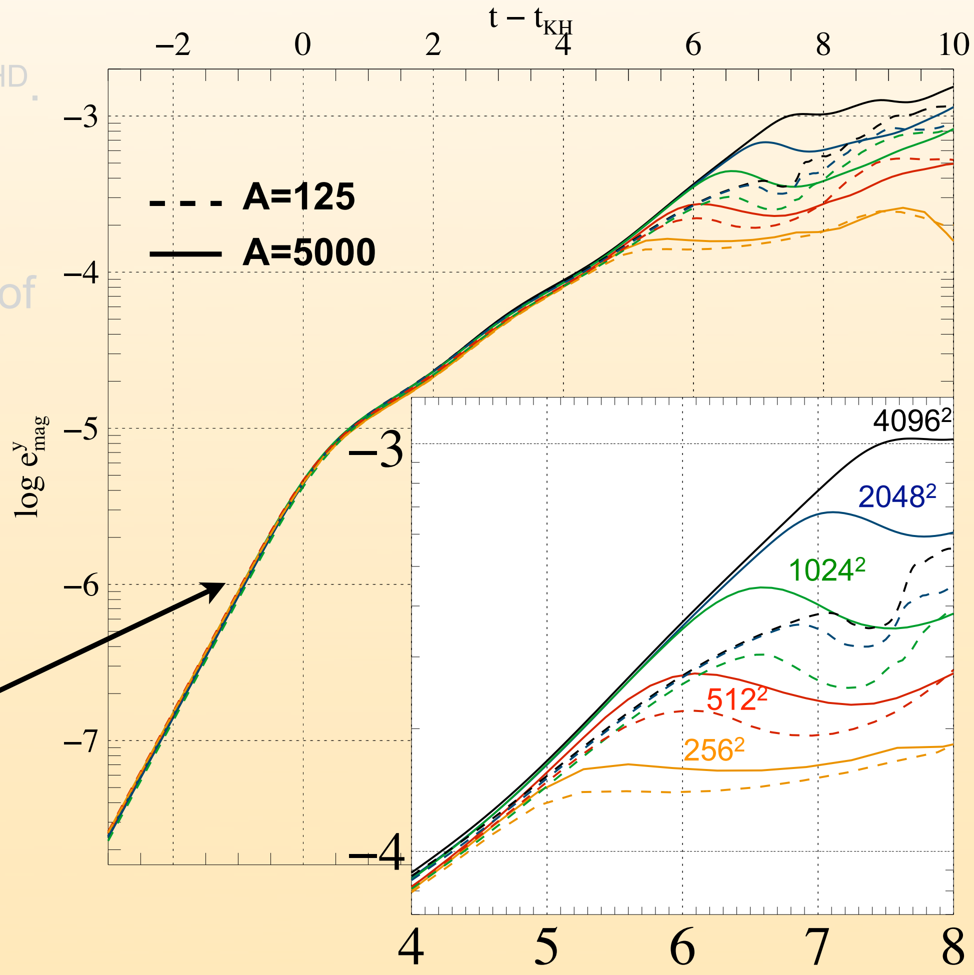

The energy of the model with A=5000 scaled up by $(5000/125)^2$.

Magnetized models: weak fields
KH-phase

- Our models grow with $\Gamma_{num}^{MHD} \sim \Gamma_{num}^{HD}$.
- Passive field amplification.
- Fixed amplification factor by the end of this phase (model independent):

$$|B|_{KH} \sim 1.4\ |B_0|$$

- By the end of the KH-phase:

$$e_{mag}^{y} \sim 0.1 \times e_{mag}$$

- Γ_{num} independent of resolution.
- Termination of the KH-phase: the vortex forms and e_{kin}^{y}, e_{mag}^{y} saturate.

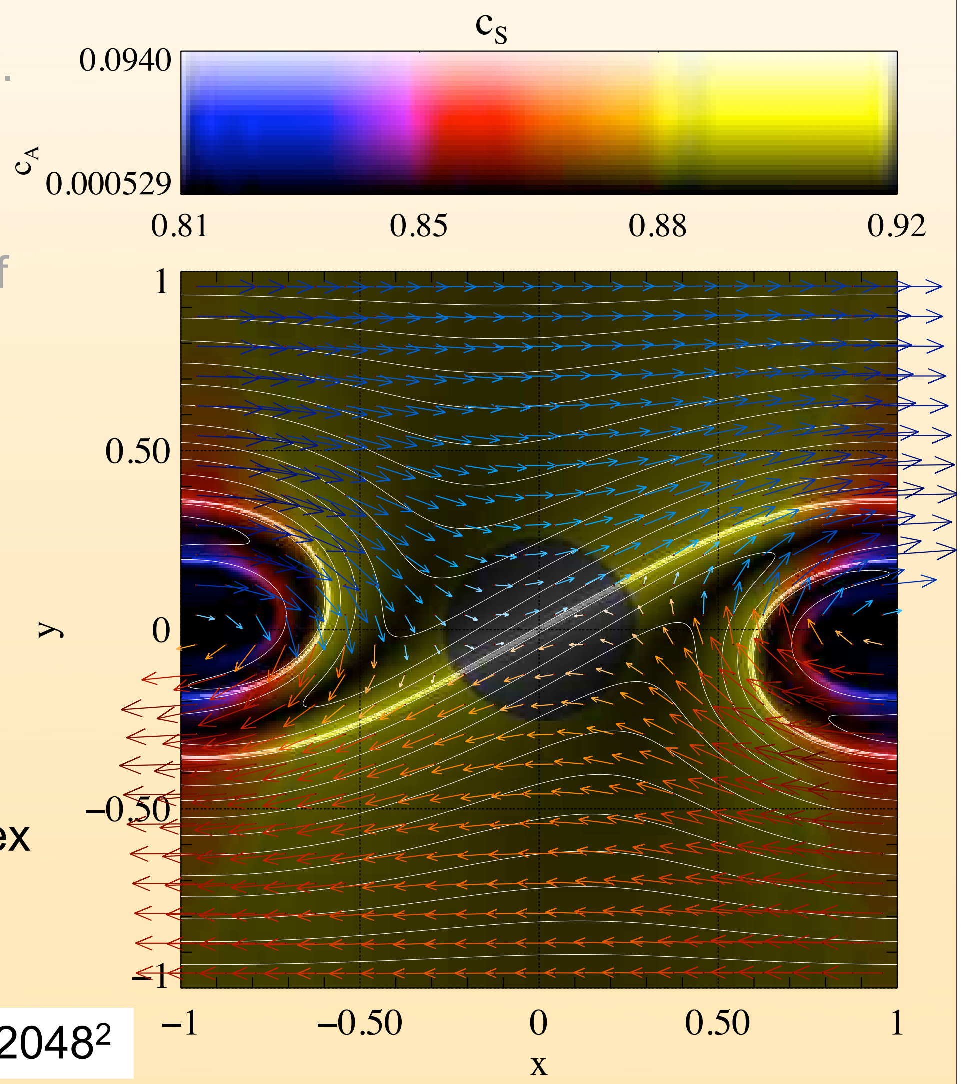

A=125, M=1, 2048^2

Magnetized models: weak fields Kinematic Amplification phase

- After the termination of the approx. hydrodynamic KH-phase, e_{kin}^{y}, saturates.
- The B-field still grows exponentially because it is wound up by the vortex.
- During this phase, **B** is still dynamically negligible. Thus, the growth rate of the field is roughly the same independent of A.

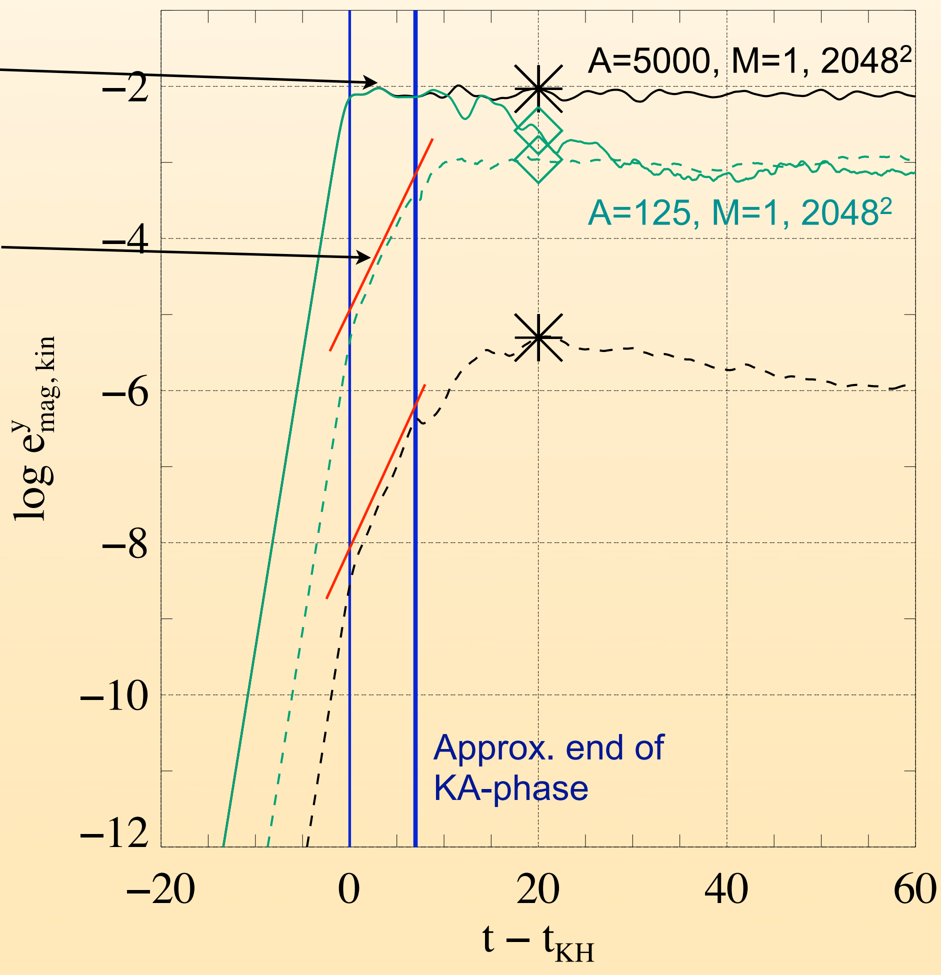

Magnetized models: weak fields
Kinematic Amplification phase

Structure of the flow before the end of the KA phase

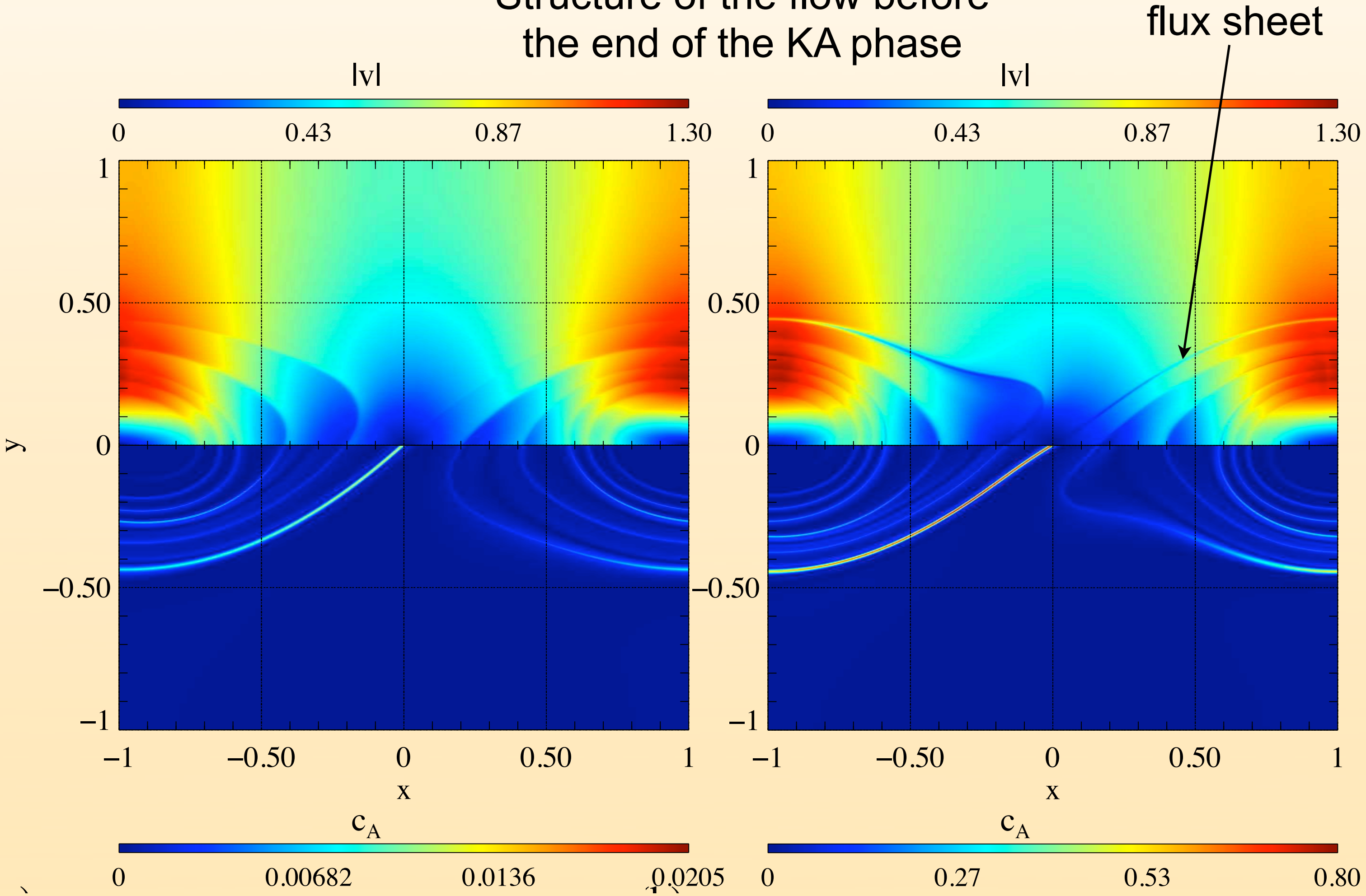

A=5000, M=1, 2048^2

A=125, M=1, 2048^2

Magnetized models: weak fields
Kinematic Amplification phase

$$\partial_t e_{\rm mag} + \nabla(e_{\rm mag}\mathbf{v}) = \underbrace{\overbrace{\cancel{-e_{\rm mag}\nabla\cdot\mathbf{v}}}^{\text{compression}} + \overbrace{b^x b^y(\partial_y v^x - \partial_x v^y)}^{\text{winding}}}_{s_{\rm mag}}$$

~ 0
(incompressible flow)

$$\partial_t e_{\rm mag} + \nabla(e_{\rm mag}\mathbf{v}) \approx e_{\rm mag} \times \mathrm{K} \longrightarrow$$ exponential amplification

- B-field grows where s_{mag}>0, i.e., predominantly along the flux sheet crossing (x,y)=0.

- The B-field amplification happens in localized, well resolved regions, thus, the growth rate is independent of resolution.

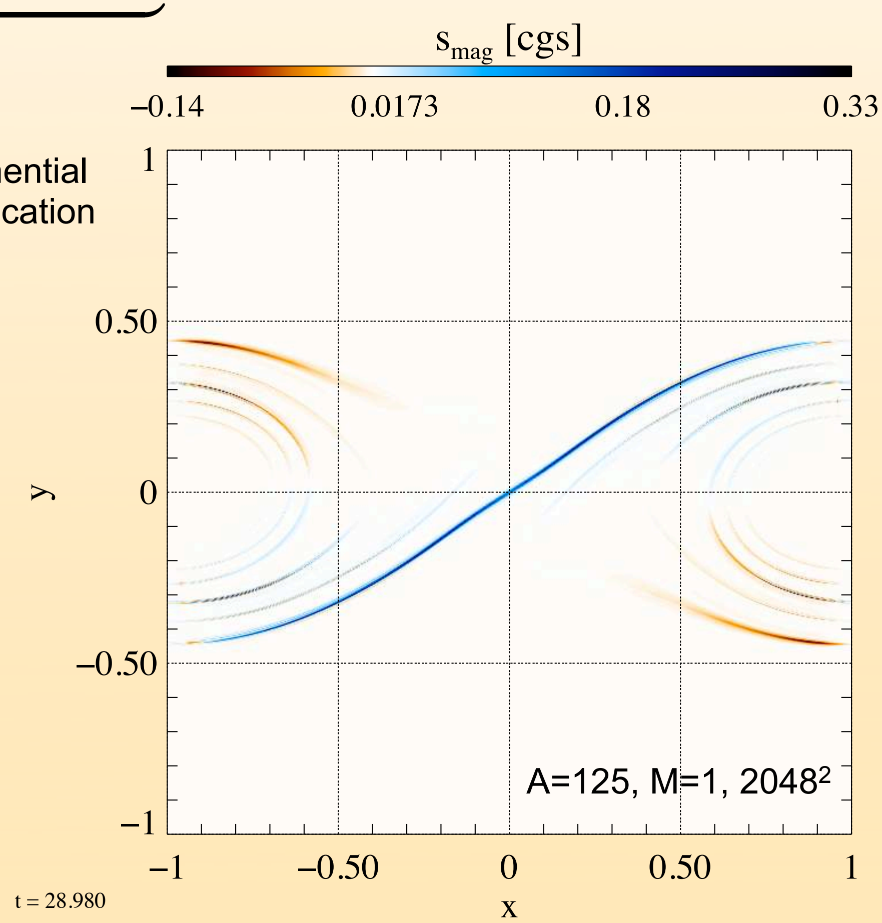

Magnetized models: weak fields
Kinematic Amplification phase

- The termination level of the KA-phase depends on resolution and on b_0.
- The growth ends slightly earlier for stronger initial fields.
- Amplification of a stronger initial field by a smaller factor than a weaker one.

- For a given m_x, there is a maximum amplification factor achieved for very small initial A.
- For a fixed initial A, f^{term} increases with increasing m_x.
- The dependence of the amplification on m_x is strong for coarse grids, but rather weak for well resolved simulations.
- For very fine resolutions (or small A), we find convergence of the Maxwell stress.

$$f^{\mathrm{term}} := \frac{M_{xy}^{\mathrm{KA}}}{M_{xy}^{\mathrm{KH}}}$$

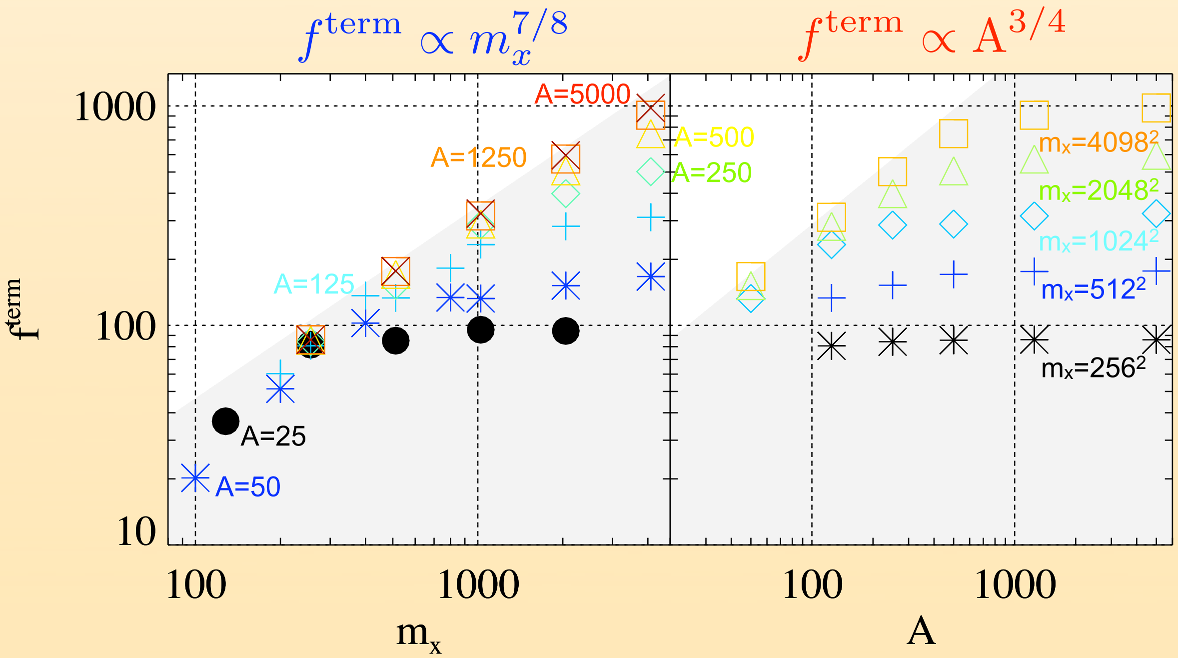

Magnetized models: weak fields
Kinematic Amplification phase

- Quantification of the resolution effects:

$$l_b = |\mathbf{b}| \,/\, |\nabla \times \mathbf{b}|$$

- B-flux conservation: l_b decreases (from $l_b \sim \infty$ @ t=0) to finite width as the field grows and winds up during the KH and KH phases.
- h=min(l_b) attainable in numerical simulations.
- If $l_b \sim h$, the B-field cannot keep growing, but e_{mag} can do it (linearly), because of the increased length of the sheet. This sets the end of the KA-phase.
- Thus, there exists $B^{max} \propto B_0 \times a\,/\,h$.
- B^{max} is only reached if the field is too weak (A<1250) to not react back on the dynamics during the KA-phase.
- At the end of the KH-phase, if A>1250, nowhere $e_{mag} > e_{kin}$, indeed, $c_A << v$.

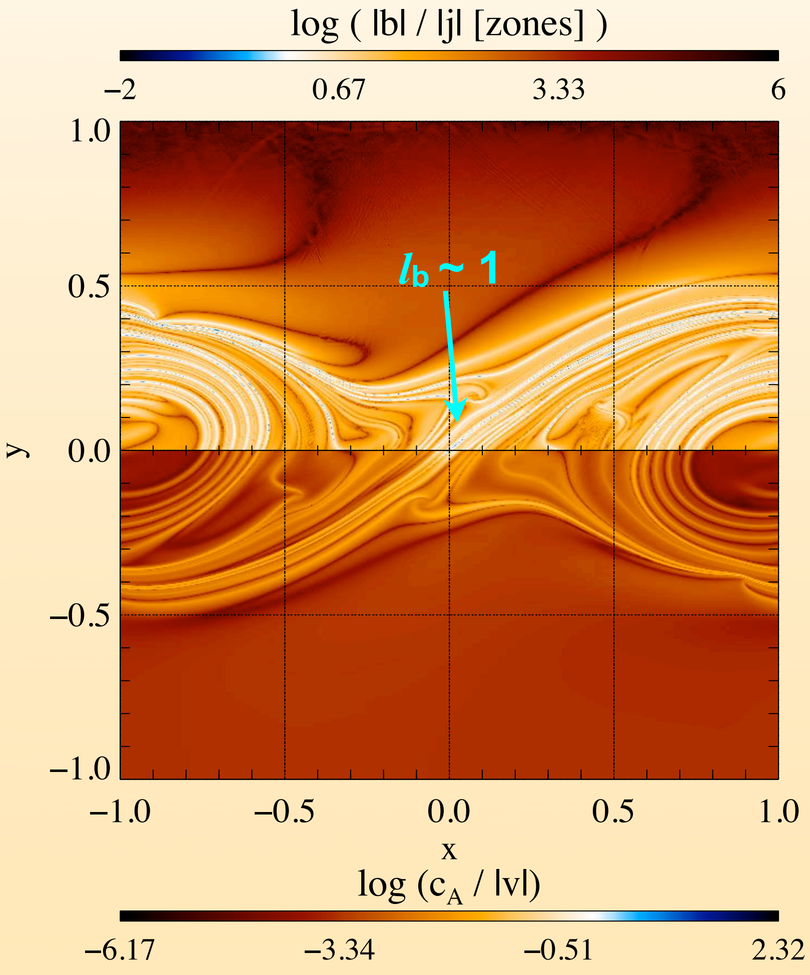

Magnetized models: weak fields Kinematic Amplification phase

- If A < 1250, because of the amplification of the B-field, it can react back on the flow, decreasing the rotational velocity of the KH-vortex, which happens if ***locally*** $e_{mag} > e_{kin}$ (or A=1).

- Numerical resistivity becomes important, but note that **because thin B-field sheets are pushed together to distances ~ h**, not because the thickness of 1 sheet ~ l_b ~ h -similar dynamics to Keppens et al 1999-.

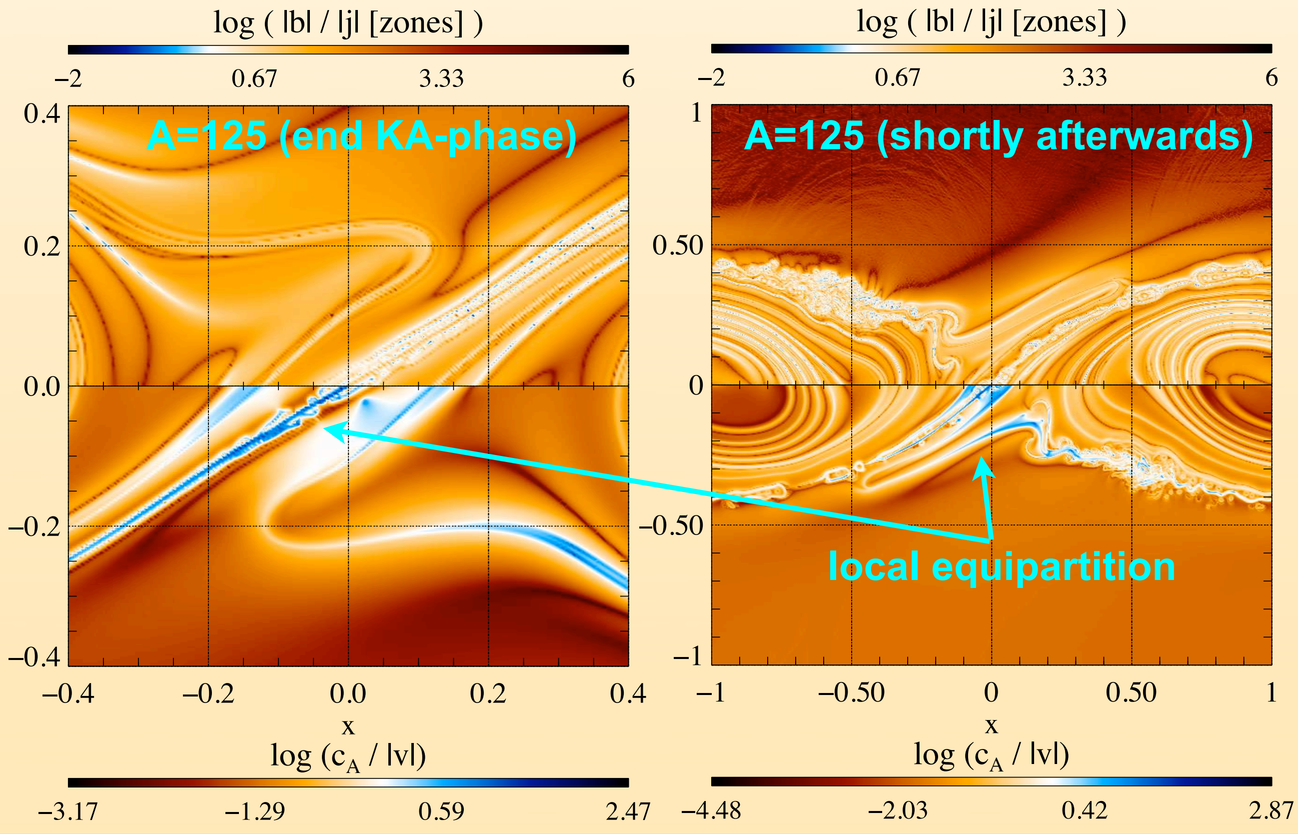

Magnetized models: weak fields
Kinematic Amplification phase

- If A < 1250, because of the amplification of the B-field, it can react back on the flow, decreasing the rotational velocity of the KH-vortex, which happens if ***locally*** $e_{mag} > e_{kin}$ (or A=1).

- Numerical resistivity becomes important, but note that **because thin B-field sheets are pushed together to distances ~ h**, not because the thickness of 1 sheet ~ l_b ~ h -similar dynamics to Keppens et al 1999-.

- This fact explains why we get numerical convergence, in contrast with the expectations for the a current sheet in a *static background* (finer grid → lower resistivity → no convergence; e.g., Biskamp 2000):
  - Instabilities terminating the growth of e_{mag} operate on a multitude of flux sheets converging due to a *dynamic background flow*.
  - Once the distance between two structures of the magnetic field becomes sufficiently small: $\Gamma_{num}^{tear} > \Gamma_{num}^{KA}$.
  - This distance is not related to the e_{mag} stored in the sheets, but it is determined by the flow field.
    - ➡ close relation: **velocity field ⇔ instance of termination**.
  - The V-field is given by the HD of the KH vortex, and does not depend strongly on resolution. Therefore:
    - ➡ The moment at which the flux sheets break up and, hence, the energy contained in them is independent on resolution.
    - ➡ **Convergence is possible despite grid-scale effects.**

Magnetized models: weak fields Kinematic Amplification phase

- Summary of the possible exits of the KH-phase:
  1. Passive termination: the field strength reaches a maximum when the flux sheets reach a thickness close to the grid spacing,
  2. Resisto-dynamic termination: a combination of dynamic and resistive termination when the field reaches local equipartition with the flow field: Lorentz forces reduce the rotational velocity of the KH vortex while resistive instabilities develop as flux sheets coalesce.
     - ➡ leads locally to A~1, independently of b_0.
     - ➡ e_{mag} increases with b_0, since B_{max}^{KA} is attained in a small patch of the volume that decreases with b_0 due to the decreasing width of the flux sheets.
- Notes:
  - Passive termination is likely a numerical artifact consequence of insufficient resolution.
  - Resisto-dynamic termination is probably the physics-wise exit of the KA-phase.

Magnetized models: weak fields
Kinematic Amplification phase

- Total amplification of the B-field (f^b) and of e_{mag} (f^e) from t=0 to the end of the KA-phase, as a function of the shear flow.
  - Increasing grid resolution ⇒ larger amplification until convergence.
  - Finer resolution needed for weaker initial fields.
  - Since $f^b \propto b_0^{-1}$ ⇒ b_{max}^{KA} independent of b_0.
  - Models with slower shear flow (smaller M) or with larger a yield smaller f^b (similar but more complex trends for f^e).

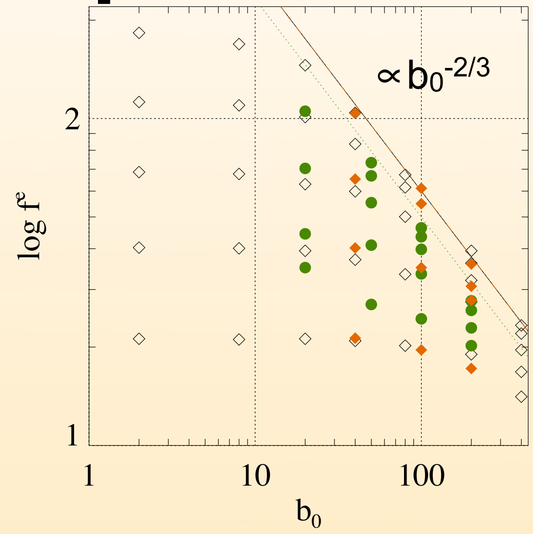

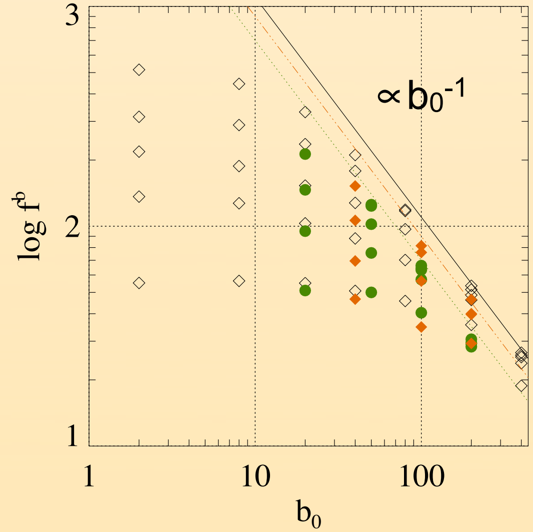

Fig. 10. The amplification factors f^e (top panel) and f^b (bottom panel) as a function of the initial magnetic field, b_0, for models with different parameters of the shear flow: empty black diamonds, filled green circles, and filled red diamonds correspond to models with M = 1 and $a = 0.05$, M = 0.5 and $a = 0.05$, and M = 1 and $a = 0.15$, respectively. The spread in vertical direction is due to different grid resolution of the simulations. To indicate the scaling with the initial field strength, we show power laws $\propto b_0^{-2/3}$ (top panel) and b_0^{-1} (bottom panel).

Magnetized models: weak fields
Saturation, dissipation and disruption

- After the end of the KA-phase, the fluid enters in a saturation phase. In the following we restrict to resisto-dynamic termination cases.
  - Secular decrease of $e_{kin}^{x,y}$ while e_{int} grows.
  - $e_{mag}^{x,y}$ stay at a roughly constant level.
  - $e_{kin}^{y} \sim e_{mag}^{y}$, but $e_{mag} << e_{kin}$.

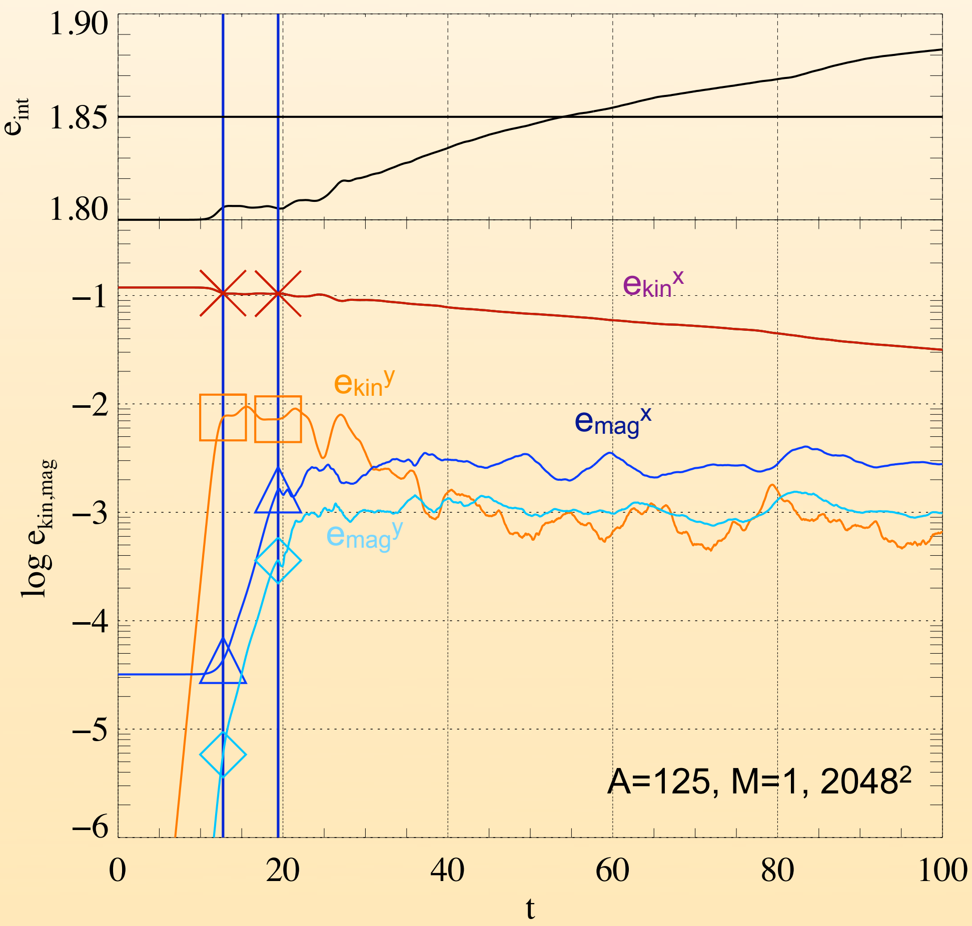

Magnetized models: weak fields
Saturation, dissipation and disruption

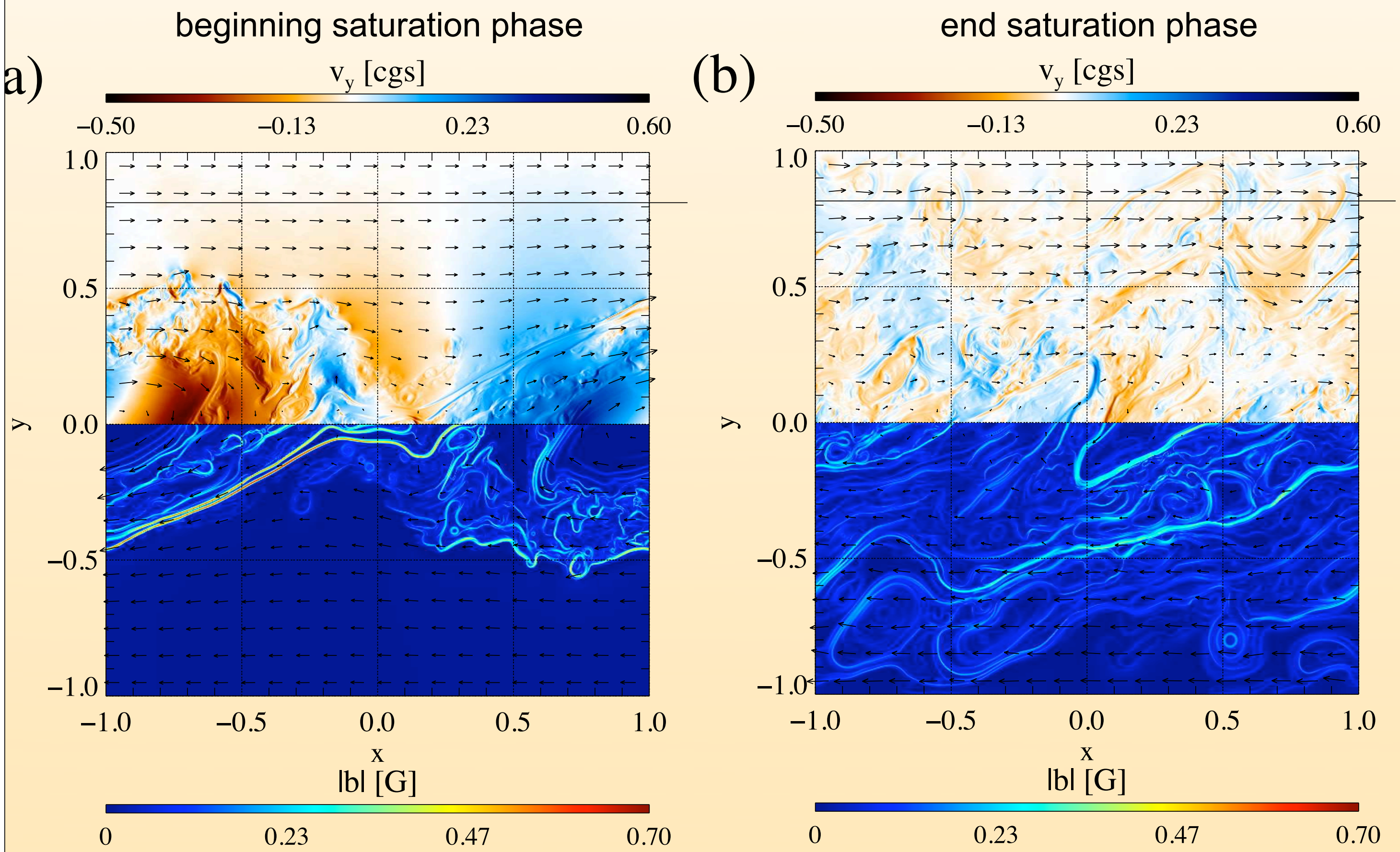

A=125, M=1, 2048^2

- Vortex disrupted.
- Broad transition layer forms.
- Magnetic field concentrated in thin sheets (l_b~ 1).
- Resistive instabilities spread all over (form, e.g., closed loops).
- B-field reaches equipartition with V-field at flux sheets. Thus, the field can greatly affect the dynamics.
- The small scale flow and field are inefficient to be amplified further.
- Steady state reached (statistical sense).

Magnetized models: weak fields
Saturation, dissipation and disruption

- *How long does it take to reach a steady state?*
- *How long does it take to decelerate the KH-vortex?*
- To quantify it, we can evaluate t_{dis}, the time it takes to reach $e_{kin}^{y} < e_{mag}$ and we define a deceleration rate as: $\sigma_{\rm dec} := \partial_t \log e_{\rm kin}^{x} = 1/t_{\rm dec}$

- We find $t_{dis} \propto b_0^{-0.7}$ and $t_{dec} \propto b_0^{-0.7}$. This will allow us to obtain typical time scales in merger motivated simulations.

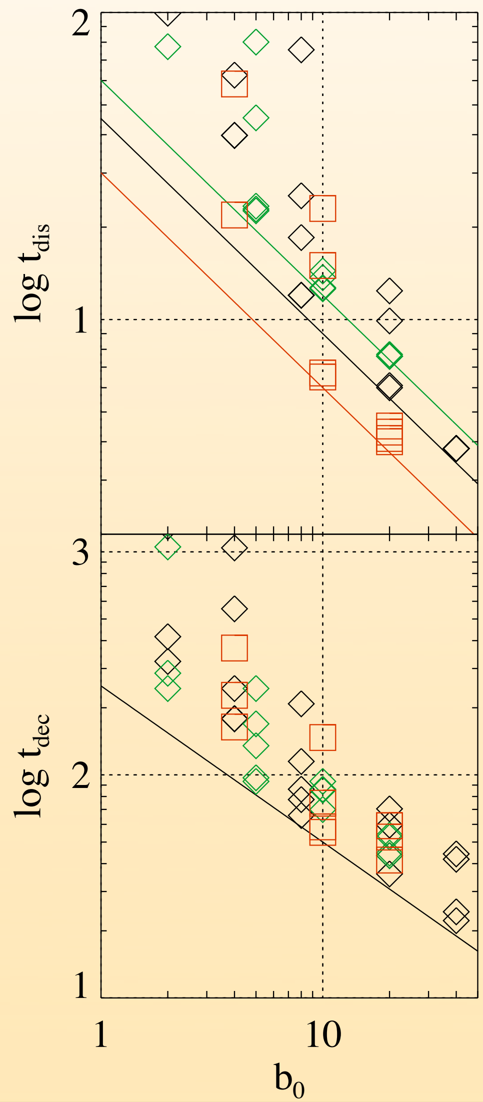

Fig. 13. The disruption of the KH vortex, $t_{\rm dis}$ (upper panel), and the deceleration time scale, $t_{\rm dec}$ (lower panel), as a function of the initial field strength, b_0. In both panels, we show in addition to the models represented by symbols, lines $\propto b_0^{-0.7}$ which show the approximate scaling of the time scales with b_0. Black diamonds, green diamonds, and red squares correspond to models with M = 1 and a = 0.05, M = 0.5 and a = 0.05, and M = 1 and a = 0.15, respectively. The scatter in the vertical direction is due to different grid resolutions of the simulations. For the same value of b_0, finer resolution yields smaller values of $t_{\rm dis}$ and $t_{\rm dec}$.

3D models: subsonic shear flows, parallel field

Nonmagnetic models:

- [Ryu et al. (2000)] the KH vortex is unstable against (purely) HD instabilities: coherent vortex tubes near the main KH vortex exert non-axial stresses on the vortex, and fluid elements are prone to the *elliptic instability*, an instability caused by time-dependent shear forces, which fluid elements feel as they orbit the vortex on elliptic trajectories. **The result is isotropic decaying turbulence**. We verify this result

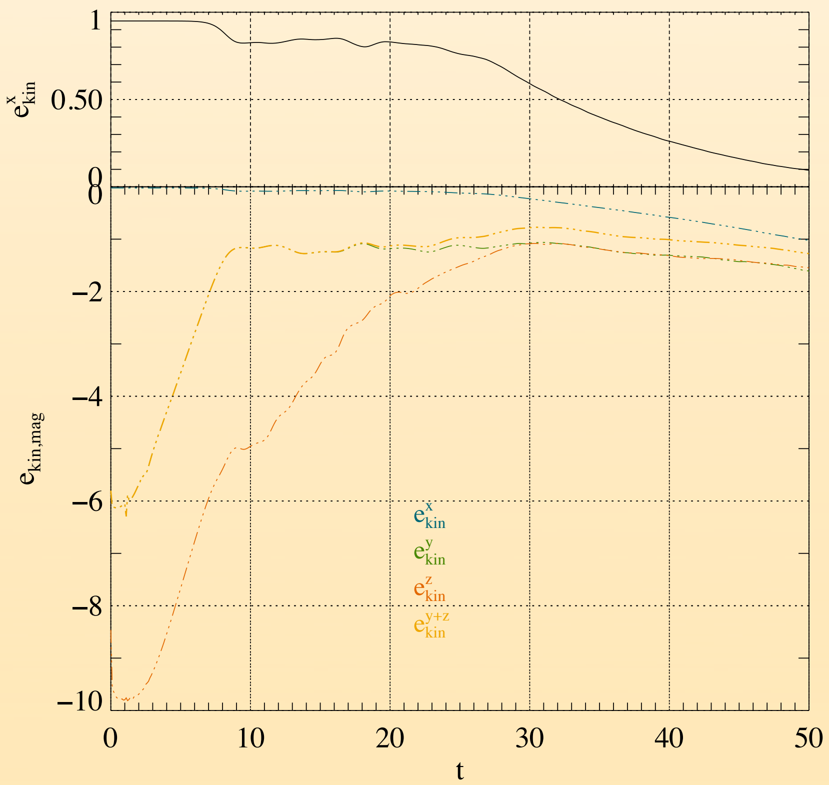

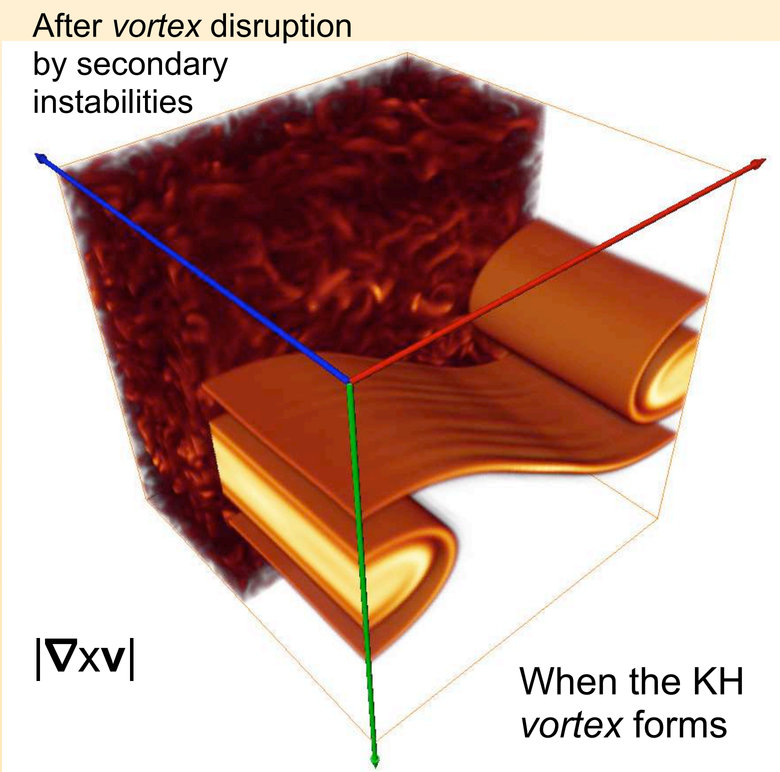

3D models: subsonic shear flows, parallel field

Weakly magnetized models:

- [Ryu et al. (2000)] If a (weak) magnetic field is present and disrupts the vortex, the post-disruption flow shows a larger degree of organization than without magnetic fields due to the prevalence of flux tubes and sheets in which the magnetic and kinetic fields are aligned. We verify this result.

There are similar evolutionary phases as in 2D, but complicated by the development of parasitic instabilities

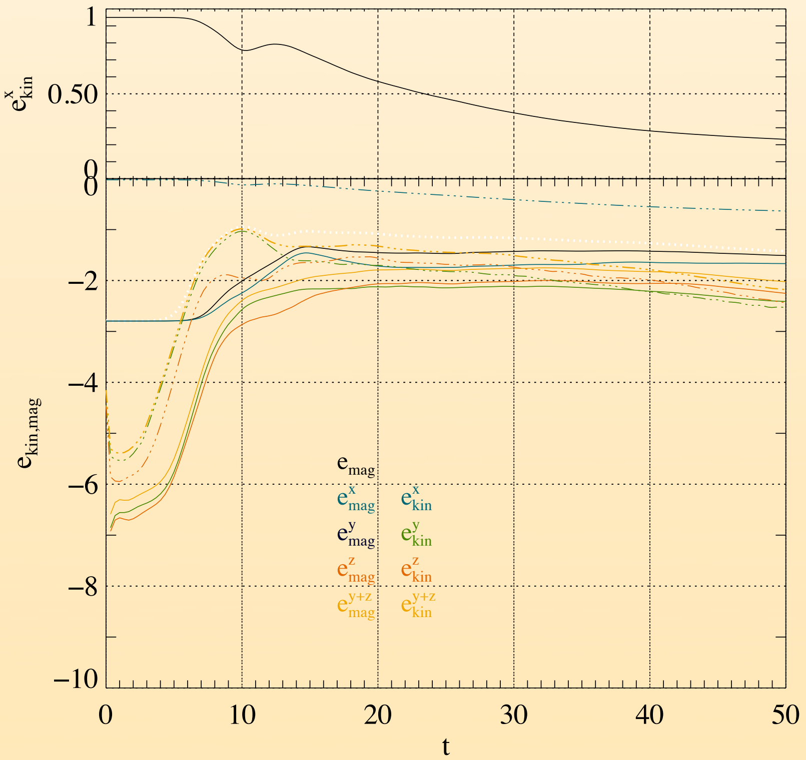

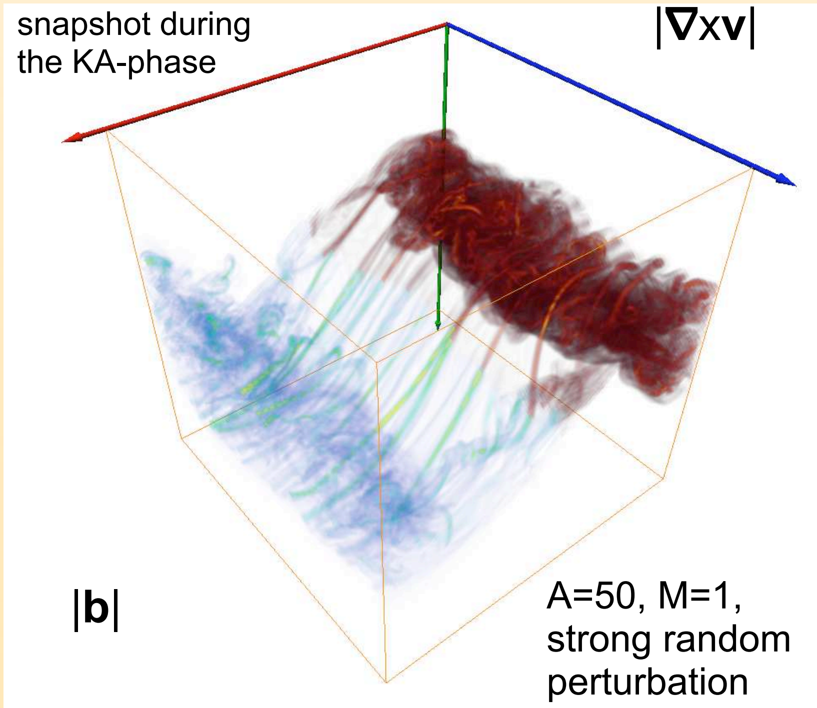

3D models: subsonic shear flows, parallel field

Weakly magnetized models:

- There is a competition between HD and MHD instabilities. Which one of the two dominates depends on A and on the initial amplitude of random perturbations. The final turbulent state can be rather different.

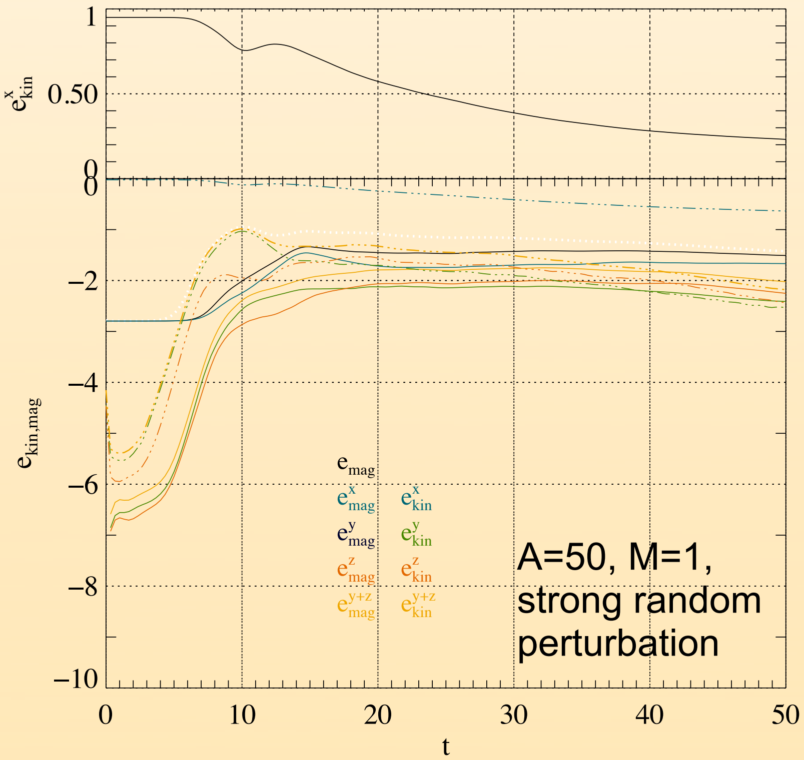

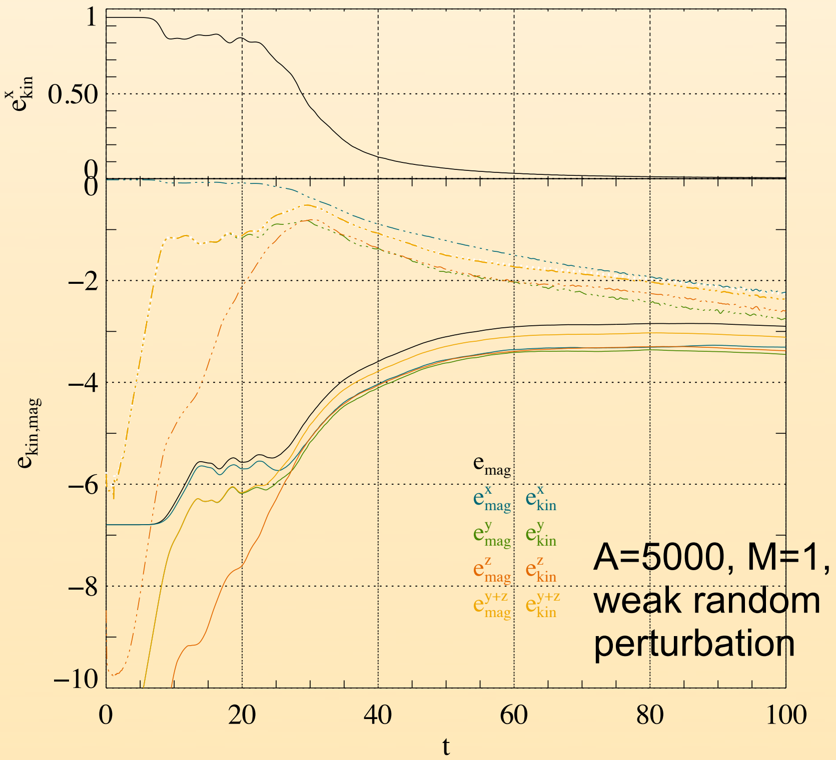

3D models: subsonic shear flows, parallel field

Weakly magnetized models:

- There is a competition between (3D) HD and (2D) MHD instabilities. Which one of the two dominates depends on A (also resolution) and on the initial amplitude of random perturbations. The final turbulent state can be rather different.
  - Hydrodynamic disruption:
    - If too weak amplification of the magnetic field leads to a dominance of HD instabilities over MHD instabilities during the early phases, the KH vortex tube is disrupted and the shear flow is decelerated at a rate similar to the non-magnetic case.
    - The magnetic field will then be amplified or sustained in the turbulent velocity field the HD instabilities yield.
    - The evolution of this class of models tends towards isotropic decaying turbulence.
    - $e_{kin}^{z} > e_{mag}$ after reaching saturation.
  - Hydromagnetic disruption:
    - The B-field leads to the disruption of the KH vortex tube before the HD instabilities can set in.
    - The deceleration of the shear flow is driven by B-fields. σ_{dec} similar to that of 2D-flows; it may, however, also be smaller depending on the MHD turbulence.
    - The turbulent final state of such models is dominated by *a strong b_x roughly in equipartition with v_x*.
    - The transverse components of both vector fields are considerably weaker.
    - $e_{kin}^{z} < e_{mag}$ after reaching saturation.

Merger motivated models: physics, initial and BCs

EoS:

- Keil et al. (1996):

$$
\begin{aligned}
P &= P_{\rm th} + P_{\rm b}, \\
P_{\rm b} &= \kappa \rho^{\Gamma_{\rm b}}. \\
P_{\rm th} &= (\Gamma_{\rm th} - 1)\varepsilon_{\rm th},
\end{aligned}
$$

$$c_s^2 = \frac{\Gamma_{\rm b} P_{\rm b} + \Gamma_{\rm th} P_{\rm th}}{\rho}$$

where the thermal energy, $\varepsilon_{\rm th}$ is defined by

$$\varepsilon^{\rm th} = \varepsilon - \varepsilon_{\rm b}.$$

$\Gamma_b = \Gamma_{th} = 1.333$

(relativistic, degenerate matter)

Initial conditions:

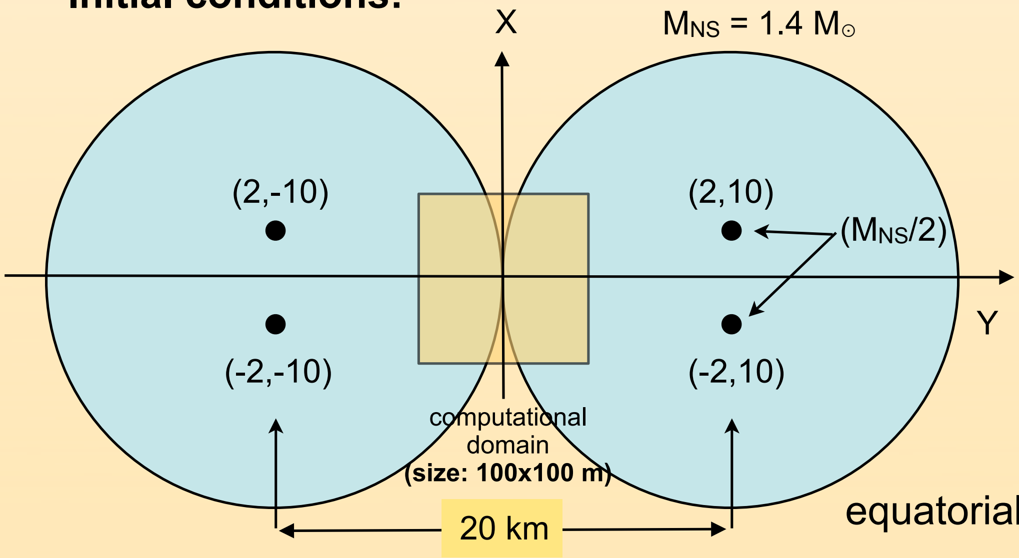

equatorial plane

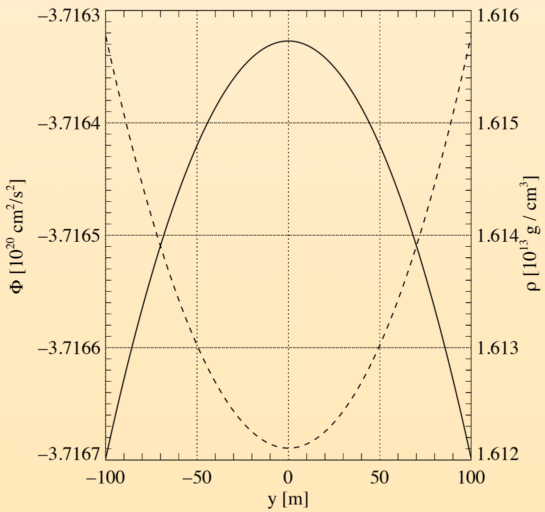

$\rho = 10^{13}$ gr/cm^3

$\varepsilon_{th} = 0$

Assume hydrostatic equilibrium

Merger motivated models: physics, initial and BCs

EoS:

• Keil et al. (1996):

$$
\begin{aligned}
P &= P_{\rm th} + P_{\rm b}, \\
P_{\rm b} &= \kappa \rho^{\Gamma_{\rm b}}. \\
P_{\rm th} &= (\Gamma_{\rm th} - 1)\varepsilon_{\rm th},
\end{aligned}
$$

$$c_s^2 = \frac{\Gamma_{\rm b} P_{\rm b} + \Gamma_{\rm th} P_{\rm th}}{\rho}$$

where the thermal energy, $\varepsilon_{\rm th}$ is defined by

$$\varepsilon^{\rm th} = \varepsilon - \varepsilon_{\rm b}.$$

$\Gamma_{\rm b} = \Gamma_{\rm th} = 1.333$

(relativistic, degenerate matter)

Initial conditions:

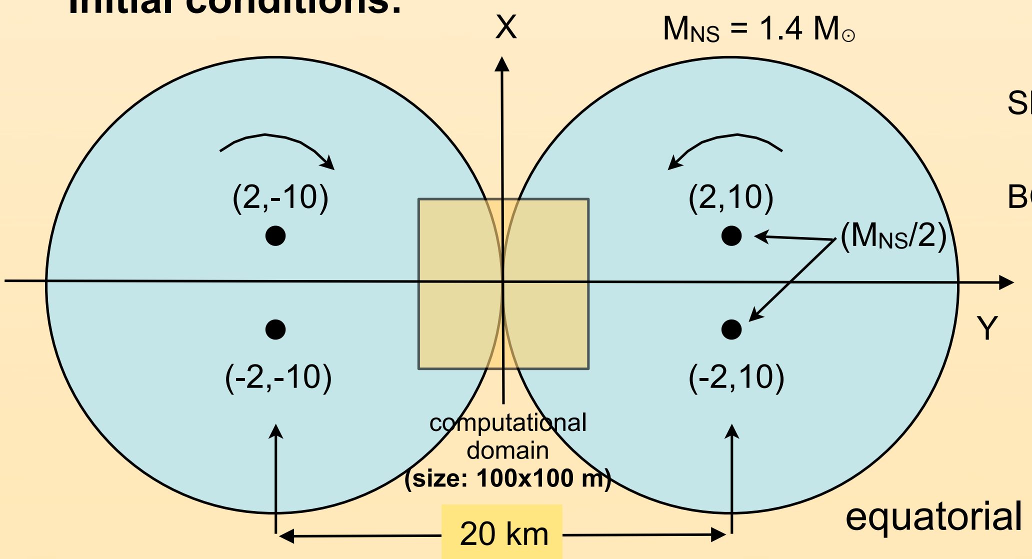

equatorial plane

Shearing velocity = rotational velocity of the NSs

BCs: x(z)-direction: periodic, y-direction: reflection

$\rho = 10^{13}$ gr/cm^3

$\varepsilon_{\rm th} = 0$

Assume hydrostatic equilibrium

Merger motivated models: 2D

- Reproduce the basic features shown in the dimensionless simulations (phases, saturation, dynamics, etc.).
- We use Cartesian grids with $l_x \times l_y = 200 \times 200$ m, resolutions up to 2048^2, a=10 m, $v_0^x = 1.83\times10^9$ cm/s =0.061c, M=0.9.
- Because of the limited grid resolution, we use $b_0 \sim 10^{14}$ G or A~115 (10^{14} G / b_0), with configurations parallel or antiparallel w.r.t. the SL.
- Find:
  - the KH vortex develops in less than **0.05 ms**, with a wavelength ~ l_x.
  - For $b_0 \sim 5\times10^{13}$ G, 10^{14} G: $b_{max}^{KA} \sim 3\times10^{15}$ G (localized in small areas), but the r.m.s. fields are much smaller $b_{rms}^{KA} \sim 2.5\times10^{14}$ G, ~ 5×10^{14} G, respectively.
  - $t_{dec} \sim 1$ ms, e.g., for a model with $b_0 = 2\times10^{14}$ G, the deceleration is sufficiently rapid to cause a significant decay (by about an order of magnitude) of the turbulent energy within 0.5 ms.
  - The evolution of the shear layer is affected by the choice of the initial conditions in the following way:
    - Parallel initial fields have, a somewhat larger impact on the dynamics of the KH instability. In this case, the non-vanishing B-flux through the x-surfaces is conserved due to the BCs, corresponding to an effective driving force. Apart from lacking this additional driver, antiparallel magnetic fields are prone to stronger dissipation due to stronger currents at the boundaries between regions of opposite polarity.
    - Very similar evolution of the turbulent e_{mag} and e_{kin}, and comparable σ_{dec}. This is a direct consequence of the weakness of the variations of the background modeling x-direction compared to y-direction.

Merger motivated models: 3D

- Reproduce the basic features shown in the dimensionless simulations.
- We use Cartesian grids with l_x x l_y x l_z = 200 x 200 x 200 m, resolutions up to 512^2, M=1.
- Because of the limited grid resolution, we use $b_0 = 5\text{x}10^{13}$ G - $4\text{x}10^{14}$ G, with configurations parallel or antiparallel w.r.t. the SL.
- Find:
  - The instability grows rapidly: saturation occurs within less than 0.1 ms, and t_{dec} and t_{dis} << 1 ms.
  - Field amplification leads to $b_{max}^{KA} \lesssim 10^{16}$ G (localized in small volumes), but the r.m.s. fields are much smaller $b_{rms}^{KA} \sim 1.6\text{x}10^{15}$ G.

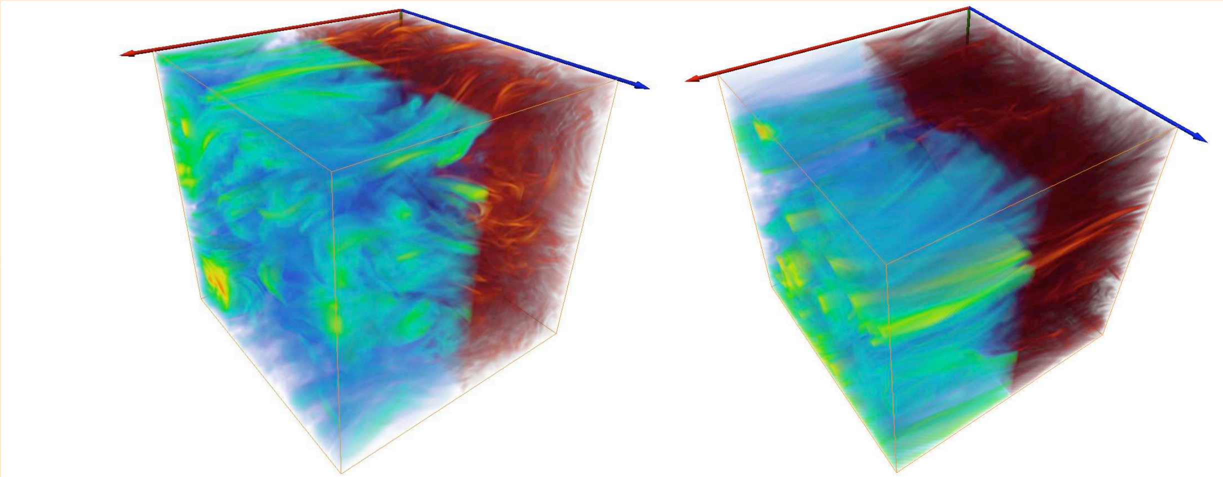

Fig. 25. The three-dimensional structure of the final turbulent state of models with $b_0^x = 5 \times 10^{13}$ G (left panel) and $b_0^x = 20 \times 10^{13}$ G (right panel) at time t = 1 ms. The plots show a volume rendering of the magnetic field strength (front half of the boxes, blue-green-yellow-red colours in an order of increasing $|\boldsymbol{b}|$) and of the enstrophy (rear half, red-yellow colours). The red, green (hidden, pointing downwards), and blue axes indicate the x-, y-, and z-directions, respectively.

Summary and conclusions (I)

Summary and conclusions (I)

- We have performed more than 300 numerical models to asses the impact of the growth of KH instabilities in the contact layer of NSs.
- The magnetic field never reaches equipartition with the internal energy (neither in its r.m.s. value nor in the local maxima). Thus B~10^{18} G are excluded from the amplification of KH perturbations in the contact layer of NSs.
- $e_{mag} \sim e_{kin}$ locally, implying $B_{max} \sim 10^{16}$ G as speculated by Price & Rosswog (2006).
- However, $B_{rms} \sim$ few x 10^{15} G, at most, thus its direct dynamical impact (deceleration of the shear flow, disruption of the KH vortex) may be rather limited.
- Both, B_{max} and B_{rms}, are even smaller if the geometry of the system and/or the merger dynamics yield a large role of HD (3D) instabilities.

Summary and conclusions (II)

Summary and conclusions (II)

- The small time scales over which B_{max} is obtained and its fast decay impose severe constraints on the impact that the amplified fields may have on any hydromagnetic or electromagnetic jet-launching mechanism in a NS-NS-merger. We note that magnetically driven relativistic outflows may need much larger time scales (~a few ms) to tap the rotational energy of either the BH or the accretion disk resulting after the merger.

- Though these results might limit the prospect for magnetic effects to play a major role in these systems, their proper inclusion to current simulations may be advantageous. Given the resolution requirements imposed by weak initial fields, a careful treatment has probably to go beyond the limit of a simple ideal MHD approach, involving, e.g., the formulation of a turbulence model for the unresolved magnetic fields.